Geochemistry Geophysics Geosystems G3
AN ELECTRONIC JOURNAL OF THE EARTH SCIENCES
Published by AGU and the Geochemical Society

Article
Volume 1
Published August 25, 2000
Paper number 2000GC000043
ISSN: 1525-2027

Self-consistent generation of tectonic plates in time-dependent, three-dimensional mantle convection simulations
2. Strain weakening and asthenosphere

Paul J. Tackley

Department of Earth and Space Sciences, University of California, Los Angeles, 405 Hilgard Avenue, Los Angeles, California 90095 (ptackley@zepher.ess.ucla.edu)

[1] **Abstract:** In a previous paper [*Tackley*, 2000b] it was shown that a combination of temperature-dependent viscosity and viscoplastic yielding is sufficient to give rudimentary plate tectonic-like behavior in three-dimensional models of mantle convection. Here the calculations are extended to include two complexities that have been suggested as being important in localizing deformation at plate boundaries: strain weakening and the presence of a low-viscosity asthenosphere. Introducing an asthenosphere by reducing the viscosity by a factor of 10 where material reaches a solidus (1) dramatically improves plate quality, even if the asthenosphere is restricted to regions around spreading centers, (2) gives good, smoothly evolving platelike behavior over a wide range of yield stress values spanning an order of magnitude, and (3) gives bimodal stable solutions over a range of yield stresses; either immobile-lid or plate behavior may be obtained, depending on initial condition. By contrast, introducing an asthenosphere by using depth-dependent viscosity has a much smaller effect on system behavior. Increasing strain weakening (1) improves localization at spreading centers but leads to an increasingly complex network of spreading centers fragmenting the plates, (2) weakens convergent zones and can make downwellings highly episodic, and (3) does not lead to pure transform boundaries in these calculations. Time-dependent "damage" evolution and instantaneous strain-rate weakening give very similar results. All cases that display platelike behavior have very long wavelength mantle heterogeneity, consistent with Earth's.

Keywords: Mantle convection; plate tectonics; rheology; lithosphere.

Index Terms: Dynamics of lithosphere and mantle; plate boundary; rheology-crust and lithosphere; tectonics.

Received January 25, 2000; **Revised** May 17, 2000; **Accepted** June 6, 2000; **Published** August 25, 2000.

Tackley, P. J., 2000. Self-consistent generation of tectonic plates in time-dependent, three-dimensional mantle convection simulations, 2, Strain weakening and asthenosphere, *Geochem. Geophys. Geosyst.*, vol. 1, Paper number 2000GC000043 [14,420 words, 15 figures, 1 table]. Published August 25, 2000.

1. Introduction

[2] The question of how plate tectonics arises from mantle convection is a long-standing puzzle, because mantle convection models or analog laboratory experiments with simple viscous, temperature-dependent rheologies do not develop plate tectonics, but rather a global stagnant rigid lid [e.g., *Christensen*, 1984b; *Ogawa et al.*, 1991; *Solomatov*, 1995; *Trompert and Hansen*, 1996]. Thus the general approach to incorporating plates in mantle convection models has been to specify some component of the system (such as surface velocities, weak zones, or faults), while solving for the dynamics of the remainder of the system [e.g., *Bunge and Richards*, 1996; *Davies*, 1989; *King and Hager*, 1994; *Zhong and Gurnis*, 1995]. It is, however, of fundamental importance to understand the formation of plate boundaries and to incorporate the relevant material properties into numerical models so that plates arise self-consistently from the constitutive equations, rather than being imposed by the modeler (for reviews, see *Bercovici et al.* [2000] and *Tackley* [2000a]). In this section, findings from previous studies are briefly reviewed, the motivation behind and features of the present model are presented, and, finally, salient aspects of lithospheric deformation are discussed.

1.1. Previous Studies

[3] Vertical two-dimensional (2-D) simulations have for some time indicated the importance of non-Newtonian rheologies in producing lithospheric weakening above upwellings and downwellings (i.e., where concentrations of stress exist) [*Christensen*, 1984a; *Cserepes*, 1982; *Kopitzke*, 1979], resulting in a rudimentary approximation of plates [*Van den Berg et al.*, 1991; *Weinstein*, 1996; *Weinstein and Olson*, 1992]. The most realistic of such models are those of *Moresi and Solomatov* [1998], which feature strongly temperature-dependent viscosity and non-Newtonian weakening using a depth-dependent yield stress intended to mimic distributed brittle deformation. Their study delineated the dependence of convective regime on yield stress, finding platelike behavior at low yield stress values, intermittent lid mobility at intermediate values, and a rigid lid at high values.

[4] Three-dimensional (3-D) geometry is fundamentally more complex than 2-D geometry, because in addition to convergent and divergent plate boundaries with their associated poloidal motion, Earth also exhibits transform (strike-slip) boundaries, which are associated with toroidal motion [*Hager and O'Connell*, 1978; *Lithgow-Bertelloni et al.*, 1993; *Olson and Bercovici*, 1991]. There are no concentrated local buoyancy forces available to drive and localize deformation at transform boundaries, so the issue of how they form has been the focus of several studies of a two-dimensional sheet representing the lithosphere, with prescribed sources of convergence and divergence [*Bercovici*, 1993, 1995]. Power-law rheology was found to be insufficient to generate narrow transform margins, even with very large values of n (the power-law index), whereas "self-lubricating" rheology, in which stress decreases with strain rate beyond a critical value, produced very sharp transform margins. Two mechanisms leading to self-lubricating rheology are the feedback between viscous dissipation and temperature-dependent viscosity [*Bercovici*, 1996] and a combination of void production during deformation and ingestion of volatiles [*Bercovici*, 1998].

[5] Only a few studies have addressed plate generation in 3-D geometry. Two studies which considered the instantaneous flow and lithospheric viscosity structure arising in a 2-D high-viscosity non-Newtonian lithospheric sheet over a 3-D constant-viscosity mantle seemed to reinforce the findings of *Bercovici*

[1998]: good plates did not form with power-law [*Weinstein*, 1998] or ductile yield stress [*Tackley*, 1998] rheologies, but they did form with a strain-rate weakening (SRW) rheology [*Tackley*, 1998] similar to the self-lubricating rheology considered by *Bercovici* [1993]. These results strongly suggested that SRW, or the time-dependent equivalent of strain weakening and time healing (SWTH), is necessary for the formation of tectonic plates, particularly transform boundaries. Further reinforcement of this notion came with the first calculation to combine temperature-dependent viscosity with viscoplastic yielding in a time-dependent 3-D calculation [*Trompert and Hansen*, 1998]; the case exhibited mainly rigid-lid convection, with occasional though tantalizing bursts of localized platelike behavior associated with part of the rigid lid collapsing into the interior.

[6] Self-consistent, time-dependent, 3-D models in which a crude approximation of plate tectonics exists and evolves continuously in space and time were presented by *Tackley* [2000b] (hereinafter referred to as paper 1). Somewhat surprisingly (because it seems to contradict the findings from previous work discussed above), this behavior was obtained using a simple yield stress, with no strain weakening being necessary. Three different types of yield strength envelope were considered: constant with depth ("ductile"), proportional to depth ("brittle"), and a combination of the two. All three descriptions gave qualitatively similar trends with increasing yield strength: distributed flow divergence at low strength, improving platelike character as yield strength is increased up to some optimum value, then erratic, episodic lid mobility, finally forming a permanent rigid lid at high strength values.

1.2. This Study

[7] While the results in paper 1 are very encouraging, the plates that were obtained are far from Earth-like. Most notably, (1) even in the best models, there was still substantial distributed surface deformation, with "plateness" values (defined later) of no more than $\sim$0.7, (2) smoothly evolving platelike behavior was found only in a narrow range of yield strength, (3) localized convergent plate boundaries (above downwellings) seemed to form more easily than localized divergent spreading centers, (4) no pure transform boundaries were observed, and (5) downwellings were generally double-sided. Thus, in this study, additional physical complexities that have been proposed as being important in the generation of localized deformation at plate boundaries are investigated.

[8] First, it has been noted that a weak asthenosphere may help promote localization of deformation (particularly at strike-slip boundaries) by decoupling the plates from the underlying mantle [*Zhong and Gurnis*, 1996; *Zhong et al.*, 1998]. Two methods of producing an asthenosphere are tried in the present paper: (1) a depth dependence of viscosity by a factor of 10 superimposed everywhere and (2) a "melting viscosity reduction" (MVR) criterion, such that in regions where the temperature reaches a solidus (a simple linear function of depth), the viscosity is reduced by a factor of 10.

[9] Second, previous plate generation studies seem to indicate that "self-lubricating" rheologies are necessary for producing focused transform plate boundaries [*Bercovici*, 1993, 1995, 1996; *Tackley*, 1998], which have generally been considered necessary for obtaining platelike behavior in three dimensions. Thus the influence of such behavior is tested here, both in the form of "instantaneous" strain-rate weakening [*Tackley*, 1998] and in the form of strain weakening and time-dependent healing, with weakening tracked by a "damage" field [*Tackley*, 2000a].

1.3. Lithospheric Rheology

[10] The emerging picture of lithospheric deformation (see *Kohlstedt et al.* [1995] for a review) consists of brittle failure in the upper 10–20 km, with ductile or semibrittle shear zones in the middle lithosphere and ductile power-law flow in the lower lithosphere and upper mantle. Lithospheric strength is roughly proportional to depth in the brittle zone [*Byerlee*, 1968] but only weakly depth dependent in the midlithosphere, although the details are not known. The strongest part of the lithosphere is the midlithosphere, which may be treated as ductily deforming; thus the ductile processes determine plate strength and may be dominant in the formation of plate boundaries.

[11] The basic strength of the lithosphere discussed above may be further decreased by weakening caused by deformation (i.e., strain weakening), which is thought to play an important role in the formation of weak, localized shear zones. Observations of microstructures from exhumed upper mantle and crustal ductile shear zones [*Drury et al.*, 1991; *Jin et al.*, 1998; *Pili et al.*, 1997; *Sorensen*, 1983; *Vissers et al.*, 1995] indicate that such shear zones are often characterized by very small grains, hydration, and elevated temperatures. Thus the possible mechanisms for their formation are thought to be grain-size reduction, volatile ingestion, and viscous heating, and various analyses have been performed to investigate how localized shear zones may form through one or more of these mechanisms [*Bercovici*, 1998; *Braun et al.*, 1999; *Fleitout and Froidevaux*, 1980; *Kameyama et al.*, 1997; *Regenauer-Lieb*, 1999; *Schubert and Yuen*, 1988; *Yuen et al.*, 1978]. Although viscous deformation is dominant at long timescales, short-timescale elastic processes may be important in forming lithosphere-scale shear zones that subsequently persist over long timescales [e.g., *Regenauer-Lieb and Yuen*, 1998].

2. Model

[12] The model is identical to that in paper 1 [*Tackley*, 2000b], with the addition of two rheological complexities. There follows a brief summary of the model, followed by a detailed discussion of the rheology.

[13] The usual nondimensional Boussinesq equations expressing conservation of mass, momentum, and continuity are assumed. Heating is entirely from within, with the core-mantle boundary (CMB) set to be insulating (zero heat flux). The temperature-based Rayleigh number Ra (based on the viscosity at temperature $T = 1$) is set to 10^5, and the internal rate H is set to 10. With this choice, internal temperatures are $\sim$1, thus maintaining a meaningful temperature scale (i.e., $T = 1$ can be thought of as the mantle potential temperature of $\sim$1600 K) and facilitating direct comparison with similar basally heated cases (not presented here) without having to rescale all of the parameters to a different nondimensionalization, as would be the case if a temperature scale based on internal heating rate were chosen [e.g., *Parmentier et al.*, 1994]. The internal heating based Rayleigh number Ra_H is thus 10^6.

[14] A periodic Cartesian domain of aspect ratio 8 is assumed, except for one case that has an aspect ratio of 16. Upper and lower boundaries are free-slip, with the top boundary isothermal ($T = 0$) and the lower boundary zero heat flux.

2.1. Rheology

[15] The key parameter in this study is "effective" viscosity, which can be a function of temperature, depth, strain rate, and strain history. The rheological model for combining these complexities is a superset of that in paper

1, in turn based on that suggested by *Tackley* [2000a].

[16] An Arrhenius-type temperature-dependent viscosity law is used:

$$\eta(T) = \exp\left[\frac{23.03}{T+1} - \frac{23.03}{2}\right], \quad (1)$$

giving a variation of factor 10^5 between nondimensional temperatures of 0 and 1. The viscosity is equal to 1.0 at $T = 1$, the "typical" internal temperature. The nondimensional activation energy corresponds to a dimensional value of ~250 kJ/mol, about half of a realistic value for olivine, and the implicit assumption of a high surface temperature (1300 K) in the above equation further reduces the viscosity variation from realistic.

2.1.1. Asthenosphere

[17] In some cases a low-viscosity "asthenosphere" is added. In order to facilitate direct comparison with purely temperature-dependent-viscosity cases, this is implemented by multiplying the temperature-dependent viscosity by some factor, rather than including an activation volume in the viscosity law, which would modify the temperature dependence. Low viscosity in the shallow mantle is introduced either by superimposing an exponential depth-dependent viscosity everywhere:

$$\eta(z,T) = \exp[2.3(0.5-z)]\eta(T), \quad (2)$$

which gives a systematic factor of 10 increase with depth, or by using a simple "melting viscosity reduction" criterion, in which the viscosity is decreased by a factor of 10 in regions where the temperature exceeds a depth-dependent solidus:

$$\eta(z,T) = \begin{cases} \eta(T) & T < T_{\mathrm{sol0}} + 2(1-z) \\ 0.1\eta(T) & T \geq T_{\mathrm{sol0}} + 2(1-z) \end{cases}. \quad (3)$$

In the above equations, z is the vertical coordinate, which varies from 0 at the CMB to 1 at the surface. The surface solidus temperature T_{sol0} is varied to give asthenospheres ranging from low-viscosity regions localized underneath spreading centers to a global low-viscosity upper mantle-like layer (except inside cold downwellings). This approximation, while crude, has the advantage of not affecting lithospheric viscosities, so that any change in behavior is certainly due to the asthenosphere.

2.1.2. Yield stress

[18] A two-component yield stress is assumed, with a depth-dependent component to represent brittle processes and a constant component to represent ductile, semibrittle processes:

$$\sigma_{\mathrm{yield}}(z) = \min[\sigma_y, (1-z)\sigma_y'], \quad (4)$$

where σ_y is the constant ("ductile") yield stress and σ_y' is the gradient of ("brittle") yield stress with depth. The yielding is implemented by means of an effective viscosity, defined as

$$\eta_{\mathrm{eff}} = \min\left[\eta(z,T), \frac{\sigma_{\mathrm{yield}}(z)}{2\dot{\varepsilon}}\right], \quad (5)$$

where $\dot{\varepsilon}$ is the second invariant of the strain rate tensor:

$$\dot{\varepsilon} = \sqrt{\dot{\varepsilon}_{ij}\,\dot{\varepsilon}_{ij}}. \quad (6)$$

2.1.3. Strain weakening

[19] Many processes are observed or inferred to weaken the lithosphere to a greater extent than the distributed faulting or pseudoplastic yielding described by (4) and (5). Examples of these include dynamic recrystallization [e.g., *Jaroslow et al.*, 1996; *Jin et al.*, 1998; *Rutter et al.*, 1999], shear heating [e.g., *Leloup et al.*, 1999; *Thatcher and England*, 1998], hydration/metamorphism [e.g., *Escartin et al.*, 1997a; D. Bercovici et al., A two-phase model for com-

paction and damage, 1, General theory, submitted to *Journal of Geophysical Research*, 1999], fault gouge development [e.g., *Marone et al.*, 1990], advection of weak material into fault zones [e.g., *Cloos and Shreve*, 1988a, 1996; *Lenardic and Kaula*, 1994; *Peacock and Hyndman*, 1999], and fluid overpressure in faults [e.g., *Sleep and Blanpied*, 1992]. Rather than focus on a particular weakening mechanism, strain weakening is here parameterized in terms of a generic damage parameter D. While this simple approach probably misses some important physics, it facilitates a useful preliminary exploration of the effects of strain weakening and history dependence as well as giving compatibility with previous studies [*Bercovici*, 1996, 1998; *Tackley*, 1998]. The damage parameter D reduces the viscosity linearly,

$$\eta_{\mathrm{eff,dam}} = (1 - D)\eta_{\mathrm{eff}}, \tag{7}$$

cannot exceed 1.0, and evolves according to the equation

$$\frac{\partial D}{\partial t} = A\underline{\underline{\sigma}} : \dot{\underline{\underline{\varepsilon}}} - H(T)D - \underline{v} \cdot \underline{\nabla} D, \tag{8}$$

where A is the production coefficient and $H(T)$ is a temperature-dependent healing rate. The above production term is appealing because it is proportional to work being done [*Bercovici*, 1993, 1998]. The temperature-dependent healing rate allows long-term memory of deformation at cold lithospheric temperatures but almost instantaneous healing at mantle temperatures. Possible limiting cases for healing rate are constant, or the inverse of diffusion creep viscosity [*Tackley*, 2000a]; here it is assumed to have the average of these (half the inverse temperature dependence of viscosity):

$$H(T) = B\exp\left[-11.52\left(\frac{1}{T+1} - \frac{1}{2}\right)\right]. \tag{9}$$

[20] The terms A and H have direct physical interpretations. H is $1/\tau$, where τ is a characteristic timescale for healing. Although this is not a well-known quantity, studies of metamorphic rocks and laboratory experiments on grain growth, etc., give an idea of how quickly the microstructure of silicates evolves. A can be related to the minimum strain necessary for substantial weakening to occur:

$$\varepsilon_{\mathrm{weakening}} \approx \frac{1}{A\sigma_{\mathrm{yld}}}. \tag{10}$$

For example, for grain-size reduction induced weakening, this may be of order unity [*Govers and Wortel*, 1995].

[21] Some of the presented calculations use the above description of strain weakening and time healing (SWTH). However, it is also useful to test the difference between this and the previously used instantaneous "strain-rate weakening" (SRW) rheologies [*Bercovici*, 1993, 1995; *Tackley*, 1998, 2000a]. The equivalent SRW rheology is derived by assuming steady state conditions:

$$\sigma_{ij} = 2\frac{\sigma_{\max}^2\eta_u}{\sigma_{\max}^2 + \eta_u^2\dot{\varepsilon}^2}\dot{\varepsilon}_{ij} \equiv 2\eta_{\mathrm{eff,dam}}\dot{\varepsilon}_{ij}, \tag{11}$$

where η_u is the "undamaged" viscosity (which may already be an effective viscosity because of pseudoplastic yielding) and

$$\sigma_{\max} = \sqrt{\frac{\eta_u H(T)}{2A}} \tag{12}$$

is the maximum possible stress, which at the reference viscosity (at $T = 1$) is simply $\sqrt{(B/2A)}$. This steady state approximation is valid if the timescale for lithospheric strength evolution is smaller than the timescale over which thermal convection evolves, or the buoyancy forces do not evolve at all, as was assumed in previous works.

[22] Using SWTH rather than "instantaneous" strain-rate weakening (SRW) also has the advantage of giving a unique viscosity at each point and time, since, in principle, SRW gives

two possible strain rate and viscosity values for each stress value, although this does not seem to have presented any problems in practice [*Tackley*, 1998].

[23] The final step in calculating the viscosity field is to truncate viscosities to be between 10^4 and 0.1, in order to avoid numerical difficulties.

2.2. Numerical Method

[24] Solutions are obtained using the finite-volume, primitive-variable multigrid code STAG3D, which is described elsewhere [*Tackley*, 1993, 1994, 1996a]. Enhancements made to deal with large viscosity variations and non-linear rheology are discussed in paper 1. A resolution of 128 × 128 × 32 cells with vertical grid refinement in the upper boundary layer was used for most cases. Resolution tests, in which calculations are performed on grids ranging from much coarser to twice as fine in each direction, are presented in Appendix A.

2.3. Diagnostics of Platelike Behavior

[25] As in paper 1, three quantitative diagnostics of platelike behavior are used: "plateness" (the degree to which surface deformation is localized), "mobility" (the extent to which the lithosphere is able to move), and toroidal:poloidal ratio. Their definitions are repeated here for completeness.

[26] Plateness P is defined as:

$$P = 1 - \frac{f_{80}}{0.6}, \tag{13}$$

where f_{80} is the fraction of the surface area in which the highest 80% of the integrated deformation occurs, deformation meaning the square root of the second invariant of two-dimensional strain rate:

$$\dot{\varepsilon}_{\mathrm{surf}} = \sqrt{\dot{\varepsilon}_{xx}^2 + \dot{\varepsilon}_{yy}^2 + 2\dot{\varepsilon}_{xy}^2}\ . \tag{14}$$

The factor of 0.6 makes P ≈ 0 for constant-viscosity, internally heated convection at $Ra_H = 10^6$.

[27] Mobility is defined as the ratio of rms surface velocity to rms velocity averaged over the entire 3-D domain:

$$M = \frac{(v_{\mathrm{rms}})_{\mathrm{surface}}}{(v_{\mathrm{rms}})_{\mathrm{whole}}}. \tag{15}$$

[28] For constant-viscosity, internally heated convection, $M \approx 1$. For the internally heated, platelike cases discussed in paper 1, M is in the range 1.2–1.3. For rigid-lid cases, M is very small.

[29] The toroidal:poloidal ratio is simply

$$R_{TP} = \sqrt{\frac{\langle v_{\mathrm{tor}}^2 \rangle}{\langle v_{\mathrm{pol}}^2 \rangle}}, \tag{16}$$

where v_{tor} is the toroidal velocity and v_{pol} is the poloidal velocity, and the mean is taken over a horizontal surface. Calculation of this ratio from the raw velocity field is not straightforward since the velocity field must first be decomposed into toroidal and poloidal components; the method for doing this was described in paper 1.

3. Results

3.1. Cases, Parameters, and Scalings

3.1.1. Yield stress profile

[30] As discussed earlier, the most realistic form of lithospheric strength profile is thought to be proportional to depth near the surface ("brittle" deformation) and approximately constant at greater depth ("ductile" deformation). It was found in paper 1 that such a composite yield stress profile gives similar results to a yield stress which is constant with depth. Thus this paper focuses mainly on the

simplest case of a yield stress which is constant with depth, although some composite-yield stress results are presented for comparison. These composite yield stress cases have a yield stress gradient $\sigma_y' = 20\sigma_y$, meaning that the upper 1/20th of the box (nominally 1/2 of the upper boundary-layer thickness) experiences the depth-proportional brittle yield stress, with the rest of the box experiencing the constant ductile yield stress.

3.1.2. Strain weakening

[31] Cases with evolving damage (i.e., strain weakening and time healing, or SWTH) are compared to cases with equivalent instantaneous strain-rate weakening. With evolving damage, $A = 0.0025$ (equation (8)), and B (equation (9)) is set to three different values, giving σ_{max} (equation (12)) of 2.8×10^3, 5.7×10^3, and 1.4×10^4 at $T = 1$. Strain-rate weakening is specified using the same σ_{max} values (equation (11)).

3.1.3. Dimensional scaling

[32] This study is performed using nondimensional parameters and variables and is at a somewhat lower convective vigor than Earth's mantle. Table 1 (reproduced from paper 1) gives a reasonable set of dimensional parameters and scalings. As discussed in paper 1, (1) assumed physical parameter values are realistic except for reference viscosity, which is at least 2 orders of magnitude too high; (2) the modeled heat flux is a factor of ~5 lower than Earth's; (3) yield stress values in this study scale to tens to hundreds of MPa; (4) a nondimensional velocity of 100 scales to ~2.5 cm/yr; and (5) simulations were run for nondimensional times of between ~0.2 and ~0.8, corresponding to scaled times of 2–8 billion years.

3.2. Melting Viscosity Reduction (MVR)

[33] Two series of cases are presented: one in which T_{sol0} (equation (3)) is changed while keeping the yield stress constant and one in which the yield stress is changed while keeping T_{sol0} constant.

Table 1. Nondimensional Quantities and Dimensional Equivalents

Quantity	non-D to	Value	Dim Value
	Assumed Quantities		
η	η_0	1	10^{23} Pa s
κ	κ	1	10^{-6} m^2/s
k	k	1	3.6 W/m/K
Length	D	1	2.89×10^6m
T	ΔT	1	1300 K
	Derived Quantities		
Heat flux	$k\Delta T/D$	1	1.62 mW/m^2
		50	81 mW/m^2
σ	$\eta_0\kappa/D^2$	1	1.2×10^4 Pa
		10^4	120 MPa
v	κ/D	1	0.001 cm/yr
		25	0.025 cm/yr
Time	D^2/κ	1	265 Gyr
		0.04	10.6 Gyr

3.2.1. Growing asthenosphere

[34] Figure 1 illustrates the effect of decreasing T_{sol0}, thereby increasing the volume of the low-viscosity asthenosphere, for a yield stress of 8.5×10^3 (scaling to a dimensional value of ~102 MPa). The viscosity fields span 5 orders of magnitude, and platelike behavior, where present, is indicated by strong (orange to red) plates surrounded by narrow weak (blue to purple) zones. Temperature isosurfaces showing cold downwellings are included both to ease interpretation of features in the viscosity plot and to give an indication of the length scale of mantle heterogeneity.

[35] With no MVR (Figures 1a and 1b, case from paper 1), "erratic" plates are obtained; that is, plate boundaries do not form a complete interconnected network, and the system is quite time dependent. A dramatic change is effected even with a fairly high $T_{sol0} = 0.8$ (Figures 1c–1f), which produces low-viscosity regions re-

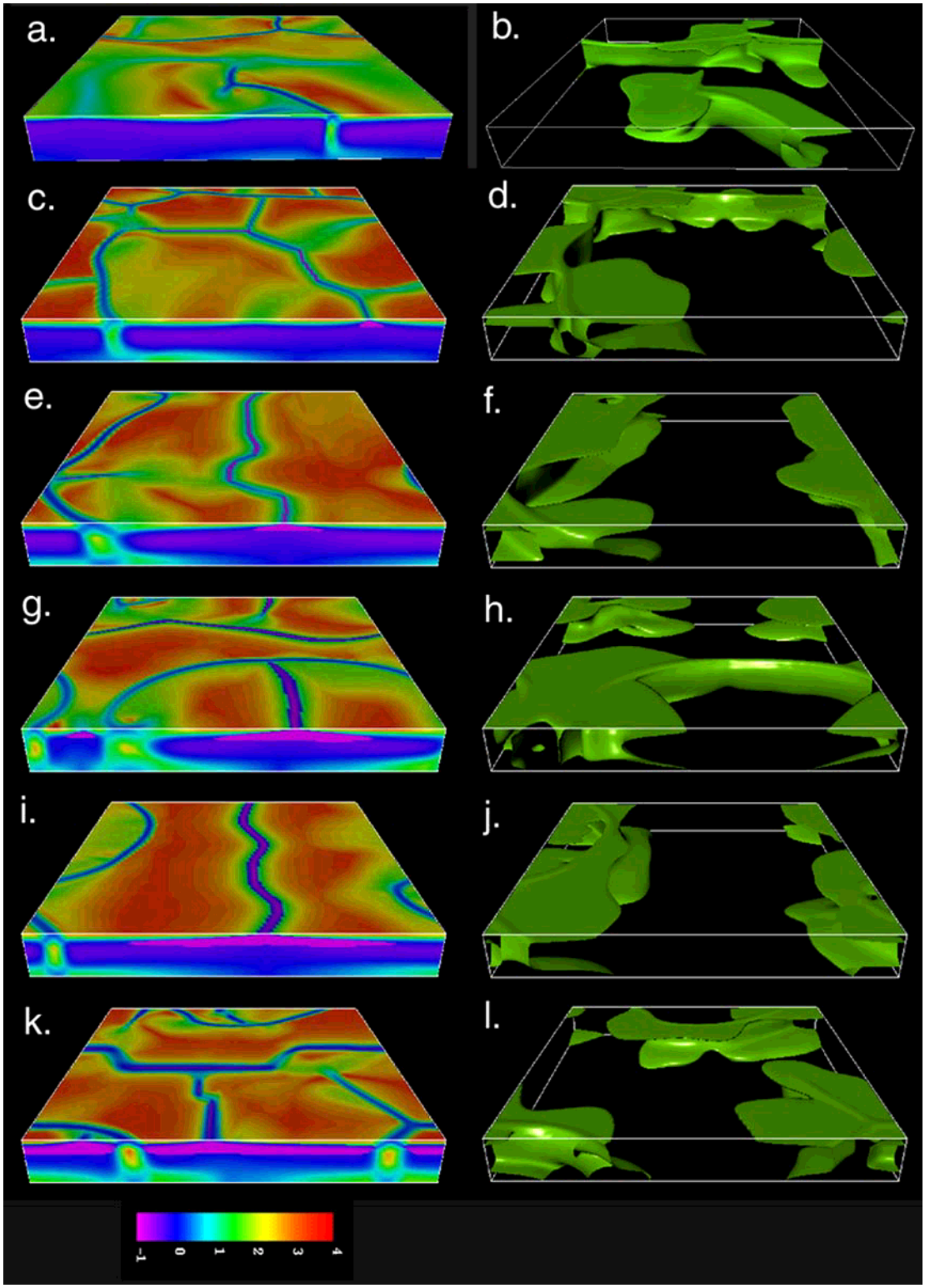
a.
b.
c.
d.
e.
f.
g.
h.
i.
j.
k.
l.
-1
0
1
2
3
4

stricted to the proximity of spreading centers (visible as purple regions in the viscosity plots). This lubrication of spreading centers greatly improves their localization, increases the effective viscosity of plates (they are mostly orange rather than being green-orange), and results in a globally complete network of plate boundaries that evolves smoothly in time. Toward the end of the simulation (Figures 1e and 1f) the system is tending toward an almost two-dimensional roll-like state. Offsets in passive spreading centers are visible, although they are not perpendicular to the spreading direction as in Earth. A decrease in T_{sol0} to 0.6 (Figures 1g–1j) results in an asthenosphere which is present under more than 50% of the lithosphere but does not seem to produce a significant further increase in plate quality; if anything, spreading centers now seem wider. Again, the system tends to a two-dimensional state toward the end. With $T_{sol0} = 0.4$ (Figures 1k and 1l) the asthenosphere is pervasive, but plate quality is not significantly improved. Some ridge offsets are visible. The temperature fields for all of these cases (right column) indicate that mantle heterogeneity is of long wavelength for all cases, even the one with no asthenosphere (Figures 1a and 1b).

3.2.2. Varying yield strength

[36] Figure 2 shows cases with depth-constant yield stress σ_y increasing from 1.4×10^3 (top row, scaling to 17 MPa) to 2.0×10^4 (bottom row, scaling to 240 MPa) for $T_{sol0} = 0.6$. Striking features of this sequence are as follows:

[37] 1. Platelike behavior (in the sense of broad, relatively strong areas being separated by narrow weak zones) is obtained over a wide, order-of-magnitude range in yield stress from 1.4×10^3 to 1.4×10^4 (17–170 MPa, illustrated in Figures 2a–2h and 2k–2n), whereas without MVR (see paper 1), platelike behavior is observed only in a narrow range of σ_y. At lower σ_y (Figures 2a–2d) the lithosphere is somewhat weak, and spreading centers become more fragmented, but between 5.7×10^3 (68 MPa, Figures 2e and 2f) and 1.4×10^4 (168 MPa, Figures 2m and 2n) there is no noticeable difference in the solution (except for Figures 2i and 2j, which were from a different initial condition).

[38] 2. In the range of σ_y from $\sim 10^4$ to 1.4×10^4 (120–168 MPa), the nature of the long-term solution (platelike versus immobile) depends on the initial condition; that is, a bimodality is observed. The $\sigma_y = 9.9 \times 10^3$ (119 MPa) case illustrates this (Figures 2i–2l). Two initial conditions were tried: (1) the "standard" one, which tends to lead to an early immobile-lid phase, and (2) the final frame of the $\sigma_y = 8.5 \times 10^3$ (102 MPa) case (Figures 2g and 2h). For $\sigma_y \geq 9.9 \times 10^3$ (119 MPa) the system cannot break out of the immobile-lid mode, once this mode is obtained. This may be due to the thick, global asthenosphere that forms beneath the lithosphere owing to high interior temperatures. However, if the system is started from a stable plate solution, it remains in this solution, changing very little over the course of the simulation. At the highest σ_y of 2.0×10^4 (240 MPa) an immobile lid is obtained regardless of the

Figure 1. Viscosity fields (left column) and temperature isosurfaces (right column) for cases with a constant yield stress of 8.5×10^3 and "melting viscosity reduction" (MVR) with varying T_{sol0}: (Figures 1a and 1b) no MVR, nominally $T_{sol0} = 1$; (Figures 1c–1f) $T_{sol0} = 0.8$, two different times; (Figures 1g–1j) $T_{sol0} = 0.6$, two different times; (Figures 1k and 1l) $T_{sol0} = 0.4$. The color bar shows log10(viscosity), which varies between 0.1 and 10,000. The horizontal viscosity slice is at $z = 0.97$. Isosurfaces show where the temperature is 0.1 lower than the geotherm.

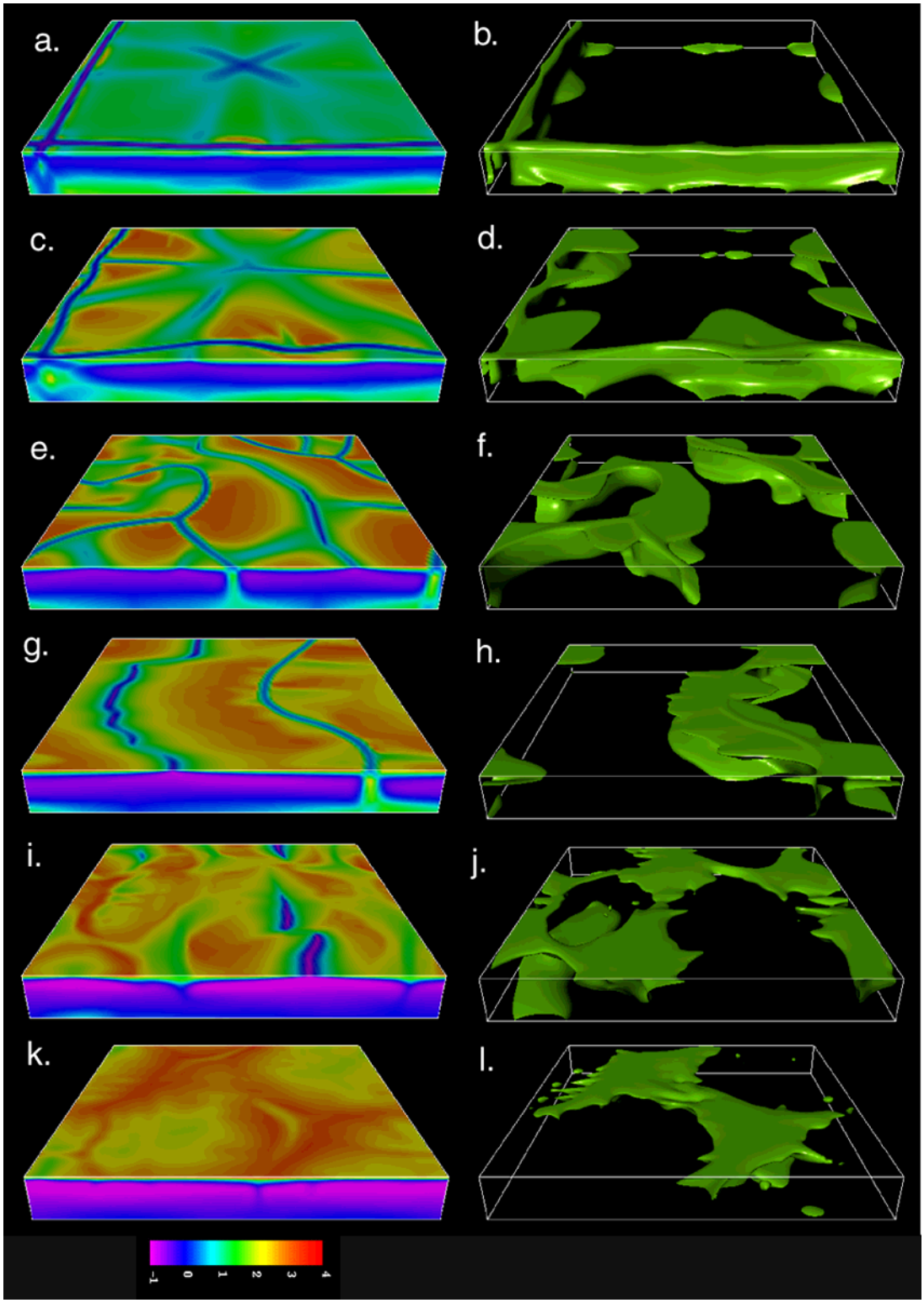
a.
b.
c.
d.
e.
f.
g.
h.
i.
j.
k.
l.
-1
0
1
2
3
4

initial condition. As with the cases reported in paper 1, the immobile lid mode obtained here is not a perfect rigid lid but is associated with very slow deformation and often long-wavelength structure below the lid. However, lid deformation is much slower than in the "sluggish lid" mode [*Ratcliff et al.*, 1997; *Tackley*, 1993]. As in paper 1, the lithospheric yield strengths which lead to platelike behavior are much lower than the strength of rocks inferred from laboratory experiments [*Kirby*, 1980].

3.2.3. Surface deformation

[39] Surface deformation for several of these cases is illustrated in Figures 3a–3e. Figures 3a–3c show the effect of increasing yield stress value over 1 order of magnitude on the quality of spreading centers: there is a trend to better localization and a smaller number of plates (i.e., larger plates). The changes in plate size are due partially to a slight rearrangement of the downwellings but mostly to a fragmentation of plates by passive rifts at low yield stresses. However, it is notable that even in the lowest yield stress case the surface deformation is still quite platelike, unlike the equivalent case with no MVR (paper 1). Differing T_{sol0} does not make a dramatic difference to the nature of surface deformation, with T_{sol0} = 0.8 (Figure 3d) giving plate behavior almost as good as that observed with T_{sol0} = 0.4 (Figure 3e) despite the huge difference in volume and coverage of asthenosphere.

3.2.4. Time dependence

[40] The time dependence both of convective quantities (rms velocity, surface heat flux, and mean temperature) and plate diagnostics (plateness, mobility, and toroidal:poloidal ratio) are shown in Figure 4. With no melting (Figures 4a and 4b) the system is very time dependent, with large swings visible in the diagnostics. Inclusion of MVR (Figures 4c and 4d) greatly stabilizes the system and leads to very good plateness, exceeding 0.9. Interestingly, R_{TP} fluctuates within a similar range for these two cases.

[41] Figures 4e–4h explore the bimodal solutions at $\sigma_y = 1.4 \times 10^4$ (168 MPa). As can be seen from the convective diagnostics, the system has reached statistically steady state by $T = 0.15$, and there is no secular trend which would suggest a change in pattern if the cases were run for longer. Immobile-lid behavior (Figures 4e and 4f) is indicated by higher convective velocities and mean temperature and by surface mobility close to zero. Platelike behavior is indicated by high values of surface mobility and plateness. At higher $\sigma_y = 2.0 \times 10^4$ (240 MPa), immobile-lid behavior is obtained even when starting from the plate solution.

[42] The rms surface velocities obtained in the platelike regime are ~130, corresponding to a dimensional value (Table 1) of 0.13 cm/yr, which, when scaled to Earth's convective regime (i.e., to the "correct" reference visco-

Figure 2. Viscosity fields (left column) and temperature isosurfaces (right column) for selected cases with viscosity melt reduction (T_{sol0} = 0.6) and varying constant yield stress, increasing from top to bottom: (Figures 2a and 2b) $\sigma_y = 1.4 \times 10^3$; (Figures 2c and 2d) $\sigma_y = 2.8 \times 10^3$; (Figures 2e and 2f) $\sigma_y = 5.7 \times 10^3$; (Figures 2g and 2h) $\sigma_y = 8.5 \times 10^3$; (Figures 2i and 2j) $\sigma_y = 9.9 \times 10^3$, standard initial condition; (Figures 2k and 2l) $\sigma_y = 9.9 \times 10^3$, started from the $\sigma_y = 8.5 \times 10^3$ case; (Figures 2m and 2n) $\sigma_y = 1.4 \times 10^4$, started from the $\sigma_y = 8.5 \times 10^3$ case; and (Figures 2o and 2p) $\sigma_y = 2.0 \times 10^4$, started from the $\sigma_y = 8.5 \times 10^3$ case. The color bar shows log10(viscosity), which varies between 0.1 and 10,000. The horizontal viscosity slice is at z = 0.97. Isosurfaces show where the temperature is 0.1 lower than the geotherm.

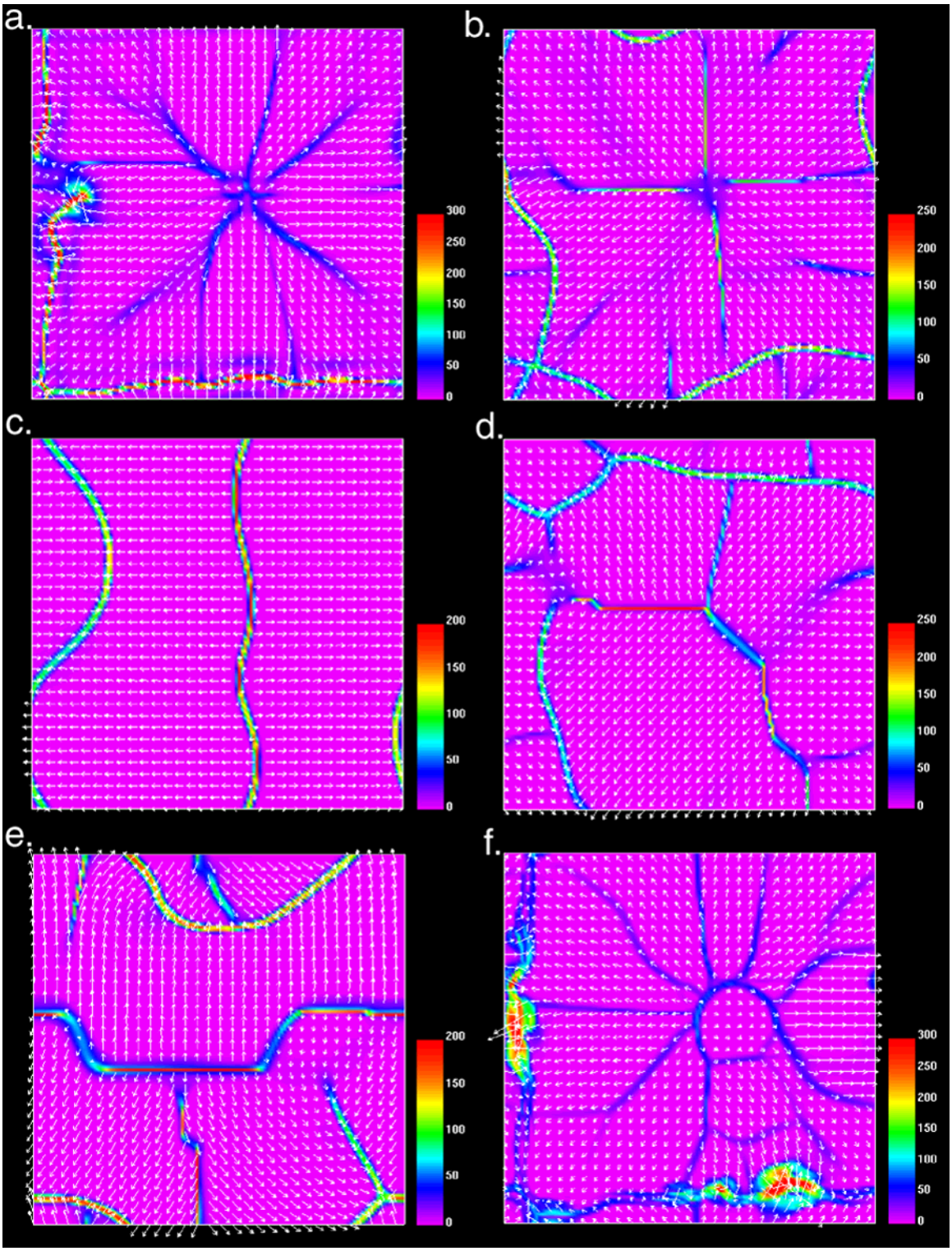
a.
300
250
200
150
100
50
0
b.
250
200
150
100
50
0
c.
200
150
100
50
0
d.
250
200
150
100
50
0
e.
200
150
100
50
0
f.
300
250
200
150
100
50
0

sity), is estimated to be 3.2 cm/yr, a realistic value.

3.2.5. Scaling of diagnostics

[43] The scalings of time-averaged diagnostics with yield stress and T_{sol0} are plotted in Figures 5a and 5b (plate diagnostics) and Figures 6a and 6b (variability of convective diagnostics). Time averaging is performed over the second half of each run, after initial transients have died down.

[44] The scaling of plate diagnostics with σ_y (Figure 5a) follows the same basic trend as the scaling observed with no asthenosphere (paper 1, here plotted as dotted lines for reference), but with several first-order differences:

[45] 1. There is much "better" plate character, as indicated most clearly by plateness, which reaches values of ~0.9, compared to ~0.7 previously. Mobility is slightly higher, but the peak value of R_{TP} is comparable with and without MVR.

[46] 2. Good plate character extends over a much wider range of yield stresses than without MVR.

[47] 3. There is a much more abrupt transition from platelike behavior to immobile-lid behavior as yield stress is increased. Without MVR the erratic, time-dependent regime exists over a range of yield stress between smoothly evolving plates and a rigid lid.

[48] 4. The final difference is the bimodal solutions discussed earlier. The scaling of plate diagnostics with T_{sol0} (Figure 5b) confirms visual impressions discussed earlier: a dramatic improvement from no MVR (nominally T_{sol0} = 1) to an asthenosphere localized to the proximity of spreading centers (T_{sol0} = 0.8) but little further improvement with additional asthenospheric volume (i.e., lower T_{sol0}).

[49] The scaling of time variability with yield stress (Figure 6a) is quite different from that obtained with no MVR (dotted lines) in two key respects. (1) Time variability is almost constant with yield stress, rather than increasing then decreasing. (2) Variations in heat flux and rms velocity are much lower (0.5–1 order of magnitude) in the yield stress range that gives optimum platelike behavior (i.e., $\sim 10^4$). The scaling of time variability with T_{sol0} (Figure 6b) confirms earlier impressions: a dramatic decrease for a small amount of asthenosphere but little additional decrease with additional asthenospheric volume.

3.3. Depth-Dependent Viscosity

[50] Cases with viscosity increasing exponentially with depth by a factor of 10 (equation (2)) are illustrated in Figure 7. The trend with σ_y appears to be similar to that observed with no depth-dependent viscosity (paper 1): good convergent boundaries but diffuse spreading centers at low yield stress (Figures 7a and 7b) and plate "quality" improving as σ_y is increased up to some optimum value (Figures 7g and 7h), above which erratic and episodic lid mobility

Figure 3. Surface velocity and strain rate fields for selected cases with constant yield stress and either melt-viscosity reduction (MVR) or evolving damage (SWTH): (Figures 3a–3c) MVR with T_{sol0} = 0.6 and increasing σ_y of 1.4×10^3, 2.8×10^3, and 1.4×10^4, respectively. (Figures 3d and 3e) $\sigma_y = 8.5 \times 10^3$ and different T_{sol0} of 0.8 and 0.4, respectively. (Figure 3f) $\sigma_y = 8.5 \times 10^3$ and SWTH with $\sigma_{max} = 2.8 \times 10^3$. Color bars show relative units (scale is truncated for Figure 3f).

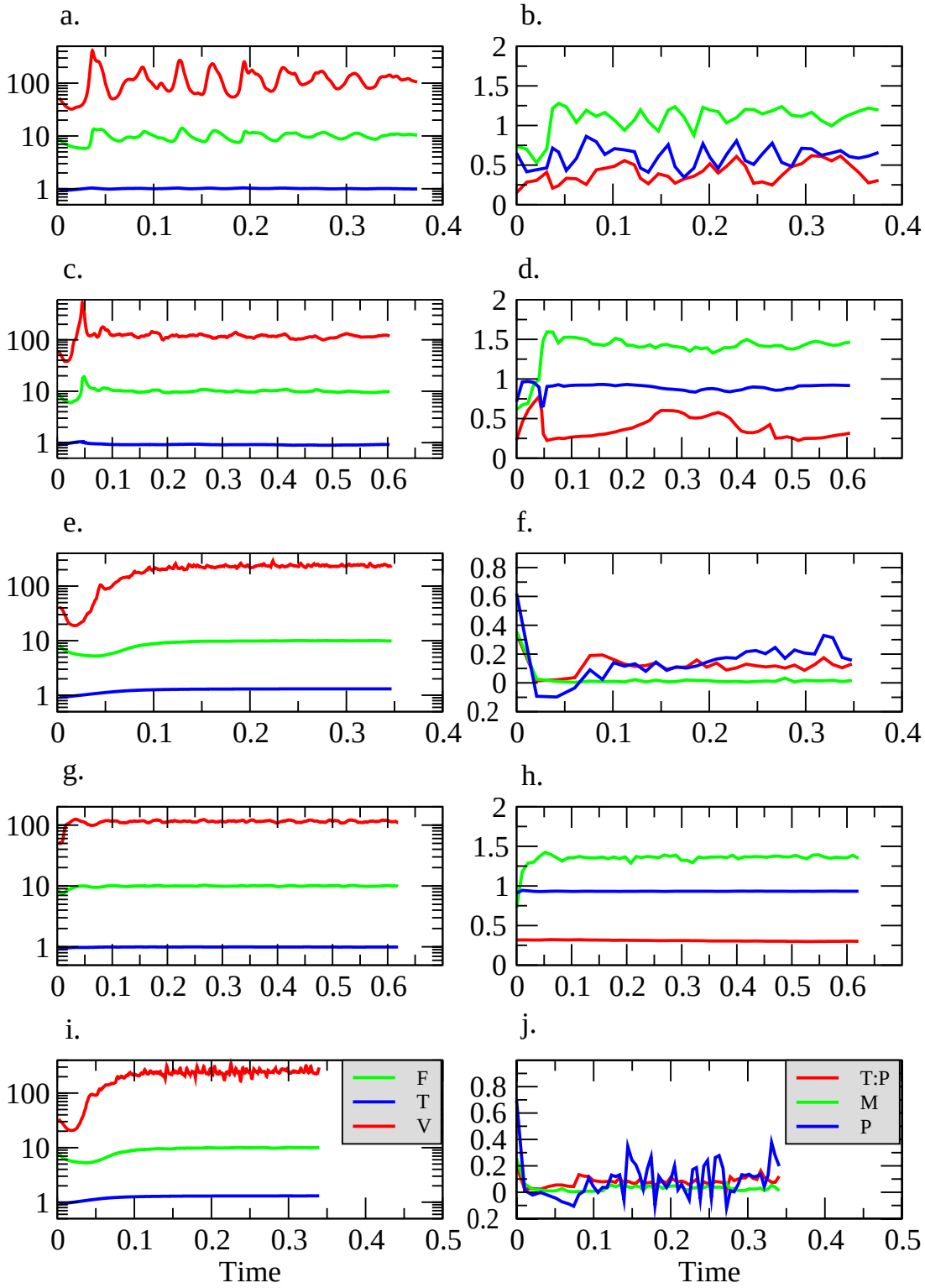
a.
b.
c.
d.
e.
f.
g.
h.
i.
j.
F
T
V
T:P
M
P
Time
Time

occurs (Figures 7i–7l). The optimum σ_y appears to be 1.3×10^4 in this series, scaling to ~156 MPa. Episodic behavior is observed even at the highest σ_y value considered here (2.8×10^4, ~336 MPa).

[51] The time dependence of these cases is illustrated in Figure 8. At low yield stress (Figures 8a and 8b) the system is very steady, but plateness and R_{TP} are low. As yield stress is increased (Figures 8c and 8d), time dependence increases, until at $\sigma_y = 1.3 \times 10^4$ (156 MPa) the system switches between episodes of low and high surface mobility (green line), although it seems to settle down in the second half of the run. At higher σ_y, extreme episodicity associated with the intermittent lid dynamics is observed.

[52] The scaling of time-averaged plate diagnostics (Figure 5c) is similar to that observed with no depth-dependent viscosity (paper 1, dotted lines) except with the regimes shifted to higher yield stress values. In addition, there is some improvement in plate quality, with plateness peaking at a slightly higher value and good platelike behavior observed over a slightly wider range of σ_y. In general, the improvement in plate quality is much less dramatic than the improvement obtained with MVR (Figure 5a). The scaling of time dependence with σ_y (Figure 6c) is again similar to the reference cases.

[53] It is thus clear that a gradual increase of viscosity with depth occurring everywhere is less effective in improving plate quality than a decrease in viscosity localized to regions near spreading centers, at least for the same amount of viscosity change (i.e., a factor of 10). This finding supports the notion that convergent plate boundaries above downwellings form more easily than passive spreading centers, and thus additional "lubrication" of spreading centers is highly effective in improving platelike behavior. Of course, Earth likely has a much larger depth variation of viscosity than that modeled here, including perhaps a jump by a factor ~30 across the 660 km discontinuity. Such a viscosity profile may reduce the need for "melt" viscosity reduction although the two things are related: the close approach of the suboceanic geotherm to the solidus may be the primary reason for the low-viscosity asthenosphere. More realistic variations of viscosity with depth, melting, and temperature must be studied in a future paper.

3.4. Strain Weakening

[54] Two sets of calculations with strain weakening are presented: one with a constant yield stress of 8.5×10^3 (102 MPa) and one with a composite yield stress of 1.4×10^4 (168 MPa, the "optimum" value found in paper 1). For each set, time-dependent strain weakening with time healing (SWTH) using evolving damage is compared with instantaneous strain-rate weakening (SRW) for equivalent parameters.

[55] Viscosity fields for the constant σ_y and composite σ_y sets are illustrated in Figure 9 and 10, respectively, with SWTH calculations

Figure 4. Time series of flow diagnostics (left column) and plate diagnostics (right column) for cases with melt-viscosity reduction ($T_{sol0} = 0.6$) and varying constant yield stress. Flow diagnostics are mean temperature (blue), surface heat flux (green), and rms velocity (red). Plate diagnostics are plateness (blue), mobility (green), and toroidal:poloidal ratio (red). (Figures 4a and 4b) Reference case with no MVR and $\sigma_y = 8.5 \times 10^3$; (Figures 4c and 4d) with MVR, $\sigma_y = 8.5 \times 10^3$; (Figures 4e and 4f) $\sigma_y = 1.4 \times 10^4$, standard initial condition; (Figures 4g and 4h) $\sigma_y = 1.4 \times 10^4$, initial condition is end of $\sigma_y = 8.5 \times 10^3$ case; and (Figures 4i and 4j) $\sigma_y = 2.0 \times 10^4$.

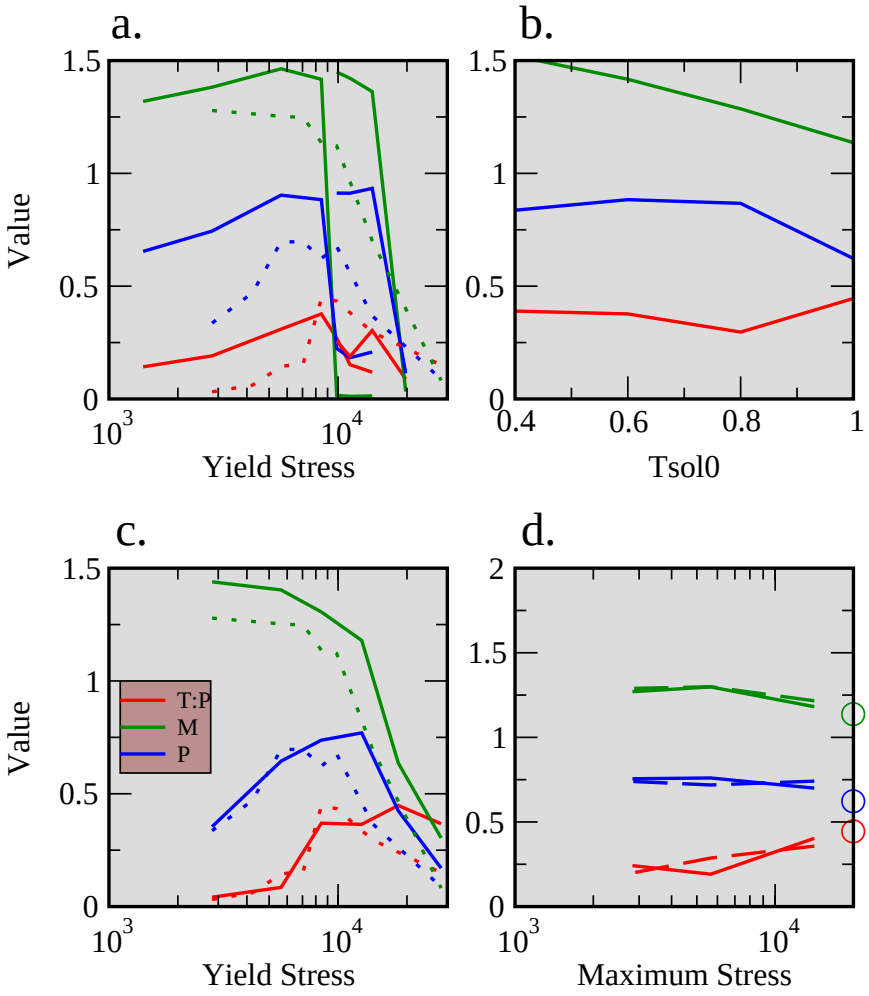

Figure 5. Scaling of time-averaged plate diagnostics toroidal:poloidal ratio (red), plateness (blue), and mobility (green) for cases with constant yield stress: (a) Scaling with yield stress for cases with melt-viscosity reduction $T_{sol0} = 0.6$. The two sets of solid curves correspond to different initial conditions (see text). The dotted curves are for cases without MVR (see paper 1). (b) Scaling with T_{sol0} for cases with MVR and $\sigma_y = 8.5 \times 10^3$. (c) Scaling with yield stress for cases with depth-dependent viscosity factor 10. Cases without viscosity increase are plotted as dotted lines. (d) Scaling with σ_{max} for cases with evolving damage (solid lines) or SRW (dashed lines) and $\sigma_y = 8.5 \times 10^3$. Values for the reference case with no weakening are plotted as circles on the vertical axis on the right-hand side.

in the left columns and SRW calculations in the right columns. Reference cases with no weakening are shown in Figure 1 (constant σ_y) and Figure 10h (composite σ_y). In both sets the same trends are visible: increased weakening (reading from top to bottom) results in weaker, better localized spreading centers, stronger plates, and weaker but more time-dependent downwellings. The spreading centers, in addition to becoming weaker, also start to form more complex, small-scale arrangements, notably in Figures 9e and 9f and Figures 10e and 10f. This complexity initially resembles cracks in a pane of glass radiating from a stone

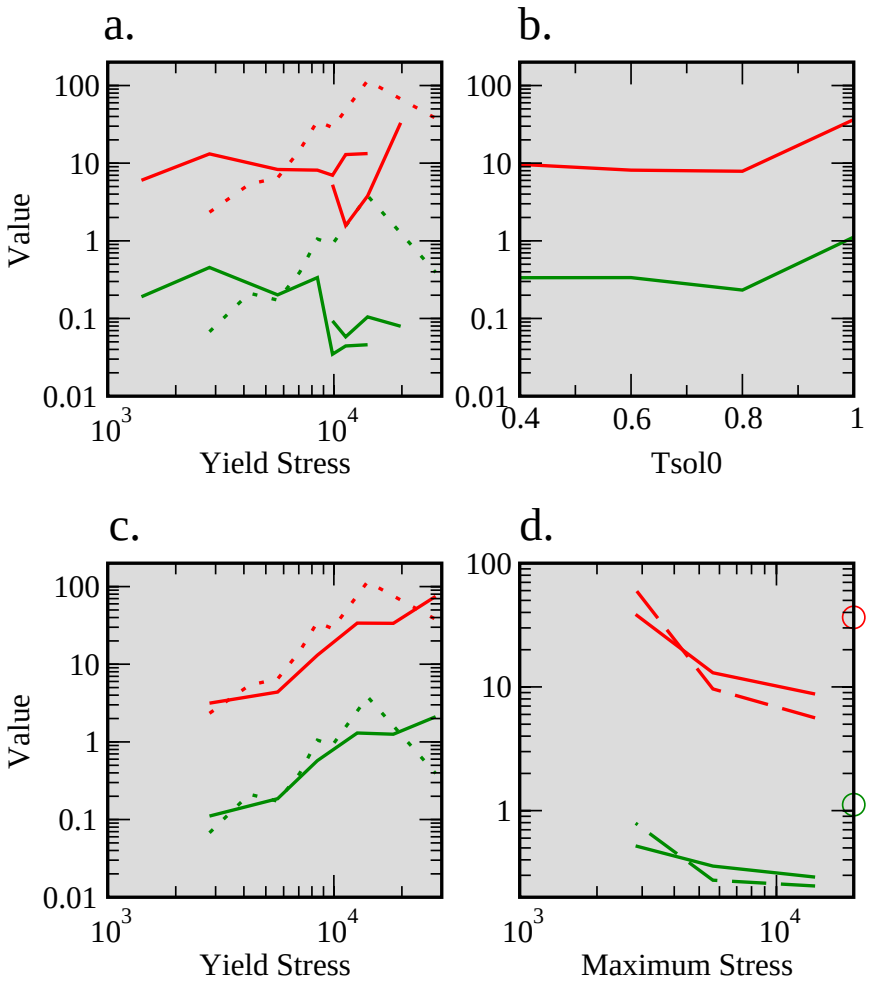

Figure 6. Scaling of time dependence for cases with constant yield stress. Time dependence is measured using the standard deviation (with respect to time) of the rms velocity (red lines) and surface heat flux (green lines). Cases are as in Figure 5: (a) Scaling with yield stress for cases with melt-viscosity reduction T_{sol0} = 0.6. The two sets of solid lines correspond to different initial conditions (see text). The dotted curves are for cases without MVR (see paper 1). (b) Scaling with T_{sol0} for cases with MVR and $\sigma_y = 8.5 \times 10^3$. (c) Scaling with yield stress for cases with depth-dependent viscosity factor 10. Cases without viscosity increase are plotted as dotted lines. (d) Scaling with σ_{max} for cases with evolving damage (solid lines) or SRW (dashed lines) and $\sigma_y = 8.5 \times 10^3$. Values for the reference case with no weakening are plotted as circles on the vertical axis on the right-hand side.

impact, although with additional weakening still more complex arrangements form. It should be noted that although these cases appear to have many small plates, the spacing of downwellings, and hence the wavelength of mantle heterogeneity, is still at the longest scale that can be fit in the box. The many small plates are caused by fragmentation of the larger plates by passive rifts.

[56] The zones of weakness surrounding downwellings become broader as the amount of weakening is increased, a trend which is accompanied by increased time dependence,

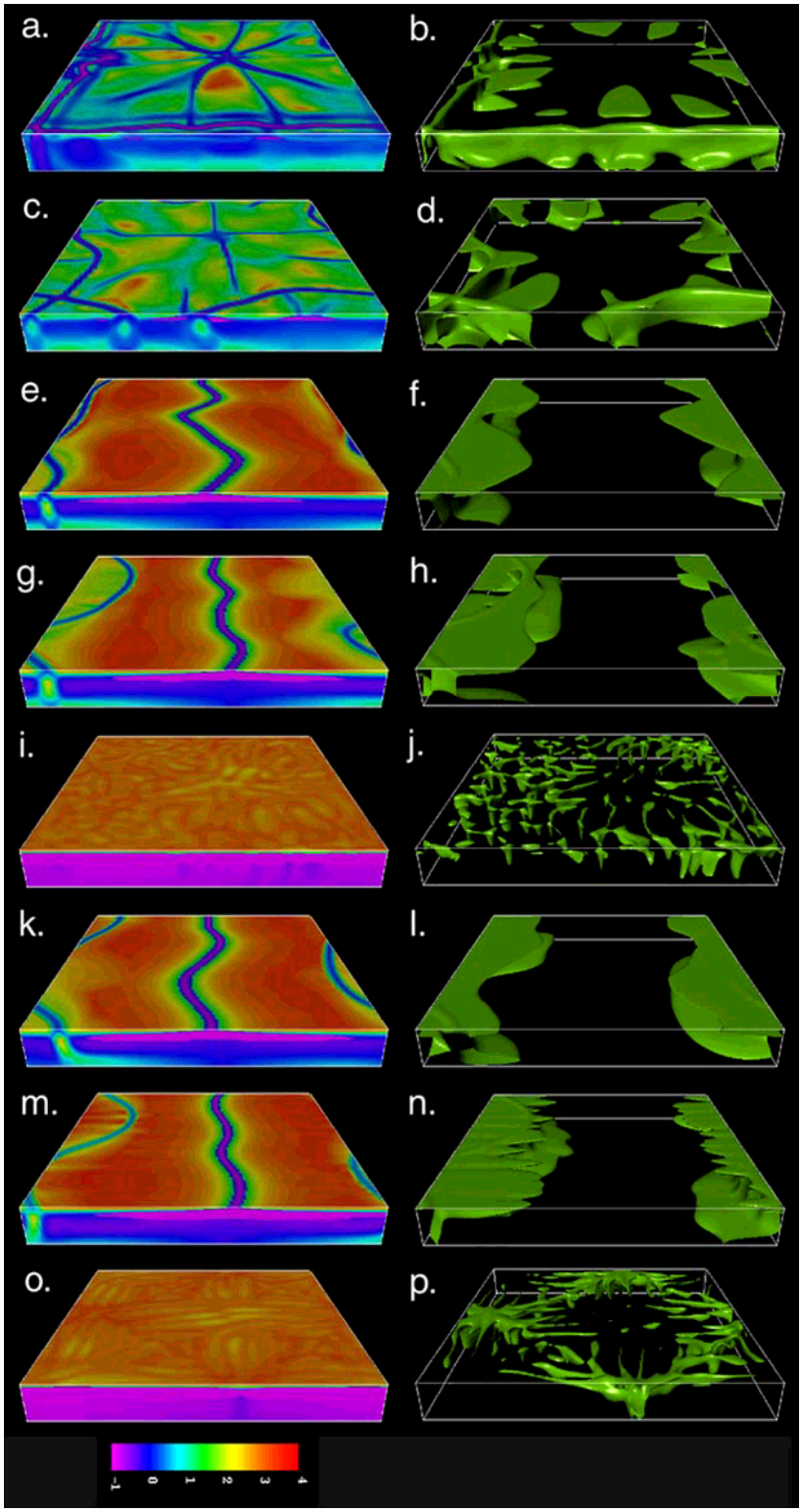
a.
b.
c.
d.
e.
f.
g.
h.
i.
j.
k.
l.
m.
n.
o.
p.
-1
0
1
2
3
4

as shown shortly. Although downwellings are still generally double-sided, the cases with intermediate SRW show an increased propensity toward single-sided downwellings. This is particularly notable in the case shown in Figure 10d, in which asymmetric downwellings exist for most of the simulation.

[57] Evolving damage (SWTH) and instantaneous SRW produce very similar results, with two main differences: (1) Additional fragmentation of spreading regions is observed with SRW, and (2) downwellings are more episodic with SRW and can undergo local "avalanches"; for example, in Figure 9f a region in the front center is collapsing into the mantle, and a weakened region extends all the way to the CMB. Of course, the absolute values of A and B (equations (8) and (9)) will affect SWTH, here described mostly in terms of σ_{max} (equation (12)), which depends only on the ratio A/B. SRW corresponds to SWTH with A and B tending to infinity while maintaining the same ratio. Other calculations (not presented here) show that as A and B are decreased while maintaining the same ratio, overall damage levels decrease, because damage requires larger strains to accumulate. This can explain the difference between the SRW and SWTH cases presented here.

[58] The surface velocity and deformation for the high-SWTH case illustrated in Figure 9e is shown in Figure 3f. The dominant features are two vigorous regional downwelling "events" in which part of the lid is collapsing into the interior. Otherwise, the deformation looks quite platelike, in the sense of having a piecewise constant velocity field, although the individual "plates" are moving in coordinated directions.

[59] Where do high levels of damage occur? Damage isosurfaces for the composite yield stress case with intermediate damage levels (Figure 10c) are shown in Figure 10g. Some damage (blue, $D = 0.1$, corresponding to 10% weakening) is observed in most regions of the lithosphere and may be advected deep into the mantle in some areas. Spreading centers experience moderate weakening (green, $D = 0.5$, 50% weakening), but the highest damage levels (red, $D = 0.9$, 90% weakening) occur around downwellings, where the material is already weak because of yielding.

[60] Time dependence of the composite yield stress, evolving-damage cases (Figure 11) indicates that small to moderate amounts of damage (Figures 11c–11f) act to steady the system compared to the case with no damage (Figures 11a and 11b). However, large amounts of weakening (Figure 11g and 11h) lead to episodic evolution, associated with regional collapses of the lithosphere surrounding downwellings. These trends are borne out by the corresponding plot of time variability versus σ_{max} (equation (12)), shown in Figure 6d. From Figure 6d it is clear that moderate amounts of strain weakening greatly reduce system time dependence compared to the reference case (plotted as circles) but that large amounts lead to even greater time variability.

[61] Does SWTH or SRW improve plate quality? Figure 5d shows how time-averaged plate

Figure 7. Viscosity fields (left column) and temperature isosurfaces (right column) for selected cases with depth-dependent viscosity (factor 10 increase) and varying constant yield stress, increasing from top to bottom. (Figures 7a and 7b) $\sigma_y = 2.8 \times 10^3$; (Figures 7c and 7d) $\sigma_y = 5.7 \times 10^3$; (Figures 7e and 7f) $\sigma_y = 8.5 \times 10^3$; (Figures 7g and 7h) $\sigma_y = 1.3 \times 10^4$; (Figures 7i and 7j) $\sigma_y = 1.8 \times 10^4$; and (Figures 7k and 7l) $\sigma_y = 2.8 \times 10^4$. The color bar shows log10(viscosity), which varies between 0.1 and 10,000. The horizontal viscosity slice is at $z = 0.97$. Isosurfaces show where the temperature is 0.1 lower than the geotherm.

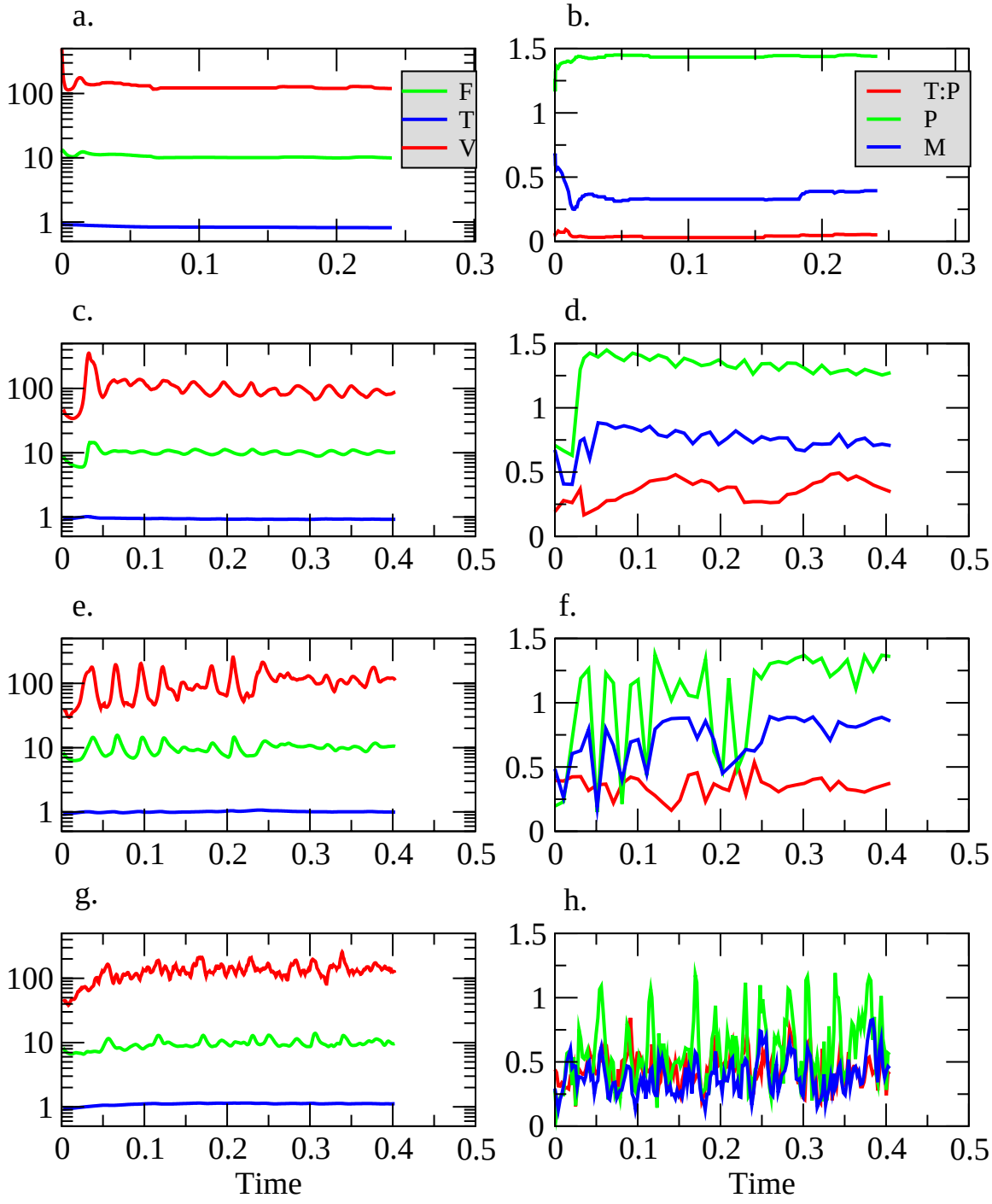
a.
b.
c.
d.
e.
f.
g.
h.
F
T
V
T:P
P
M
100
10
1
1.5
0.5
0
0.1
0.2
0.3
0.4
0.5
Time

diagnostics scale with σ_{max}, with the non-strain-weakening case plotted as circles for reference. Plateness is somewhat improved by the introduction of strain weakening, jumping from ~0.67 to ~0.75. Curiously, the toroidal:poloidal ratio decreases with increased weakening. Mobility shows a slight increase.

[62] Many of the cases seem to exhibit a planform that is strongly influenced by the shape of the box. Although, as discussed in paper 1, the chosen aspect ratio may be similar to the "effective" aspect ratio of Earth's mantle, this is of concern because the Earth's mantle is a different shape, and so it is useful to consider how things are changed if the geometrical restriction is relaxed. For this purpose, a fairly platelike case (with intermediate damage levels) was run in an aspect ratio 16 box (which is certainly a larger aspect ratio than Earth but useful for theoretical guidance). The result, illustrated in Figure 10i, seems to indicate that the character of the solution is robust but that the exact planform is influenced by domain size. Two long, arcuate subduction zones wind their way around the box, with passive rifts filling in the gaps.

3.5. Asthenosphere and Strain Weakening Together

[63] How do the two types of rheological complexity considered here interact? A brief assessment of this is obtained by presenting two cases (Figure 12) that contain both an asthenosphere and strain weakening.

[64] The first case (Figures 12a and 12b) combines a constant yield stress, melting viscosity reduction, and strain rate weakening. Compared to the equivalent case with only MVR (Figures 1g–1j), the convergent boundaries are weaker. Compared to the equivalent case with only SRW (Figures 9c and 9d), the passive spreading centers are weaker and sharper. Plateness for this frame is 0.88, no better than the case with only MVR.

[65] The second case (Figures 12c and 12d) combines a composite yield stress with depth-dependent viscosity and SRW. Compared to the equivalent case with only SRW (Figure 10b), the spreading centers are much weaker and better defined, and compared to the case with no strain weakening (Figure 10h), both spreading centers and convergent zones are improved.

[66] In summary, when an asthenosphere and SRW are combined, the asthenosphere is dominant in weakening spreading centers, while SRW provides some additional weakening of downwellings. The overall plate quality is similar to that obtained with an asthenosphere only.

3.6. Toroidal and Poloidal Flow

[67] The presented simulations display quite high R_{TP}, usually within the range observed for Earth (0.3–0.5, excluding net rotation [*Lithgow-Bertelloni et al.*, 1993], substantially higher if net rotation is included [*O'Connell and Hager*, 1991], but net rotation is not possible in periodic Cartesian geometry), despite the lack of pure transform boundaries. Paper 1 investigated the origin of this toroidal motion in terms of lid deformation, finding that all boundaries have some mixture of convergence/divergence and vertical vorticity, with toroidal motion

Figure 8. Time series of flow diagnostics (left column) and plate diagnostics (right column) for cases with depth-dependent viscosity factor 10 and varying constant yield stress. Flow diagnostics are mean temperature (blue), surface heat flux (green), and rms velocity (red). Plate diagnostics are plateness (blue), mobility (green), and toroidal:poloidal ratio (red). (Figures 8a and 8b) $\sigma_y = 2.8 \times 10^3$; (Figures 8c and 8d) $\sigma_y = 8.5 \times 10^3$; (Figures 8e and 8f) $\sigma_y = 1.3 \times 10^4$; and (Figures 8g and 8h) $\sigma_y = 1.8 \times 10^4$.

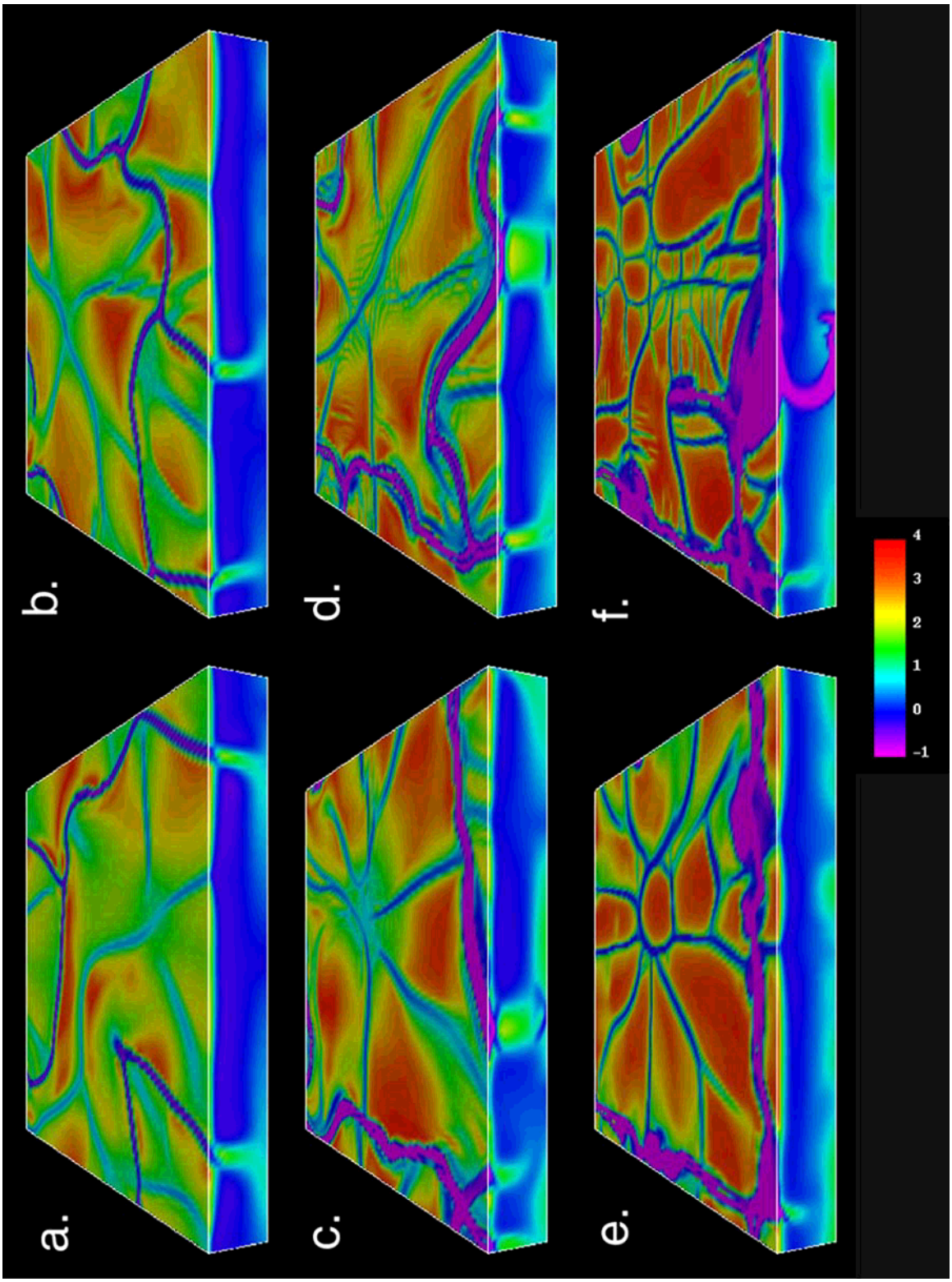
a.
b.
c.
d.
e.
f.
4
3
2
1
0
-1

associated with asymmetry in the planform. How do the additional complexities of an asthenosphere and strain weakening affect this? Figure 13 shows a decomposition of surface deformation into poloidal and toroidal components for the case with both MVR and SRW illustrated in Figures 12a and 12b. The toroidal:poloidal ratio for the illustrated frame is 0.57. As before, all plate boundaries contain a mixture of vorticity and convergence/divergence, with some plates exhibiting net rotation. However, unlike in paper 1, where regions of high vorticity were mainly focused into patches, high vorticity now occurs in smooth lines along plate boundaries, which is more realistic for Earth. Thus these additional rheological complexities result in a more Earth-like distribution of vorticity, although pure transform margins are still not obtained.

[68] How does toroidal and poloidal motion partition deeper in the mantle? The expectation from previous results [*Gable et al.*, 1991] is that toroidal motion should be maximum at the surface and decay into the mantle, particularly rapidly if the upper mantle is less viscous. This is investigated here for several cases. Figure 14 shows the depth dependence of horizontally averaged rms poloidal and toroidal velocities for several cases, calculated for representative frames.

[69] With a constant yield stress and no other complexity (Figure 14a), toroidal motion (red line) is indeed maximum at the surface and decays into the mantle, although the decay occurs mostly in a restricted range of z (0.5–0.9) and is less than a factor of 2. The poloidal motion (green line) is largest at the surface and CMB and minimum in the center of the cell. Conversely, for constant-viscosity convection (blue line), the poloidal motion is maximum in midcell and lower at the surface and CMB (toroidal motion is zero). Why this difference? At the surface and CMB the poloidal motion is horizontal, whereas in midcell the poloidal motion is mostly vertical. This difference can thus be understood as a consequence of how the aspect ratio affects horizontal and vertical convective velocities. Because of conservation of mass, wide cells (aspect ratio >1) lead to (midcell) vertical velocities that are lower than (surface) horizontal velocities, whereas narrow cells (aspect ratio <1) lead to vertical velocities that are higher than horizontal velocities. The presented platelike cases have wide cells, whereas constant-viscosity convection (presented in paper 1) has narrow "cells."

[70] Melt viscosity reduction introduces some important differences (Figure 14b). Increasing asthenospheric volume (lower T_{sol0}) causes toroidal motion to increase at the surface but decrease at depth (red→orange→magenta curves), thus producing a larger drop-off of toroidal motion with depth. At $T_{sol0} = 0.4$, toroidal motion decreases by a factor of ~4 with depth, with most of the decrease occurring in the z range 0.7–0.9, which is approximately the base of the low-viscosity region. This is consistent with the results of *Gable et al.* [1991]. Increasing astheno-

Figure 9. Viscosity fields comparing cases with evolving damage (left column) and strain-rate weakening (right column) for a constant yield stress of 8.5×10^3. Amount of damage or SRW increases from top to bottom, as indicated by "maximum" stress (equation (12)) of (Figures 9a and 9b) 1.4×10^4; (Figures 9c and 9d) $\sigma_y = 5.7 \times 10^3$; and (Figures 9e and 9f) $\sigma_y = 2.8 \times 10^3$. The color bar shows log10(viscosity), which varies between 0.1 and 10,000. The horizontal viscosity slice is at $z = 0.97$.

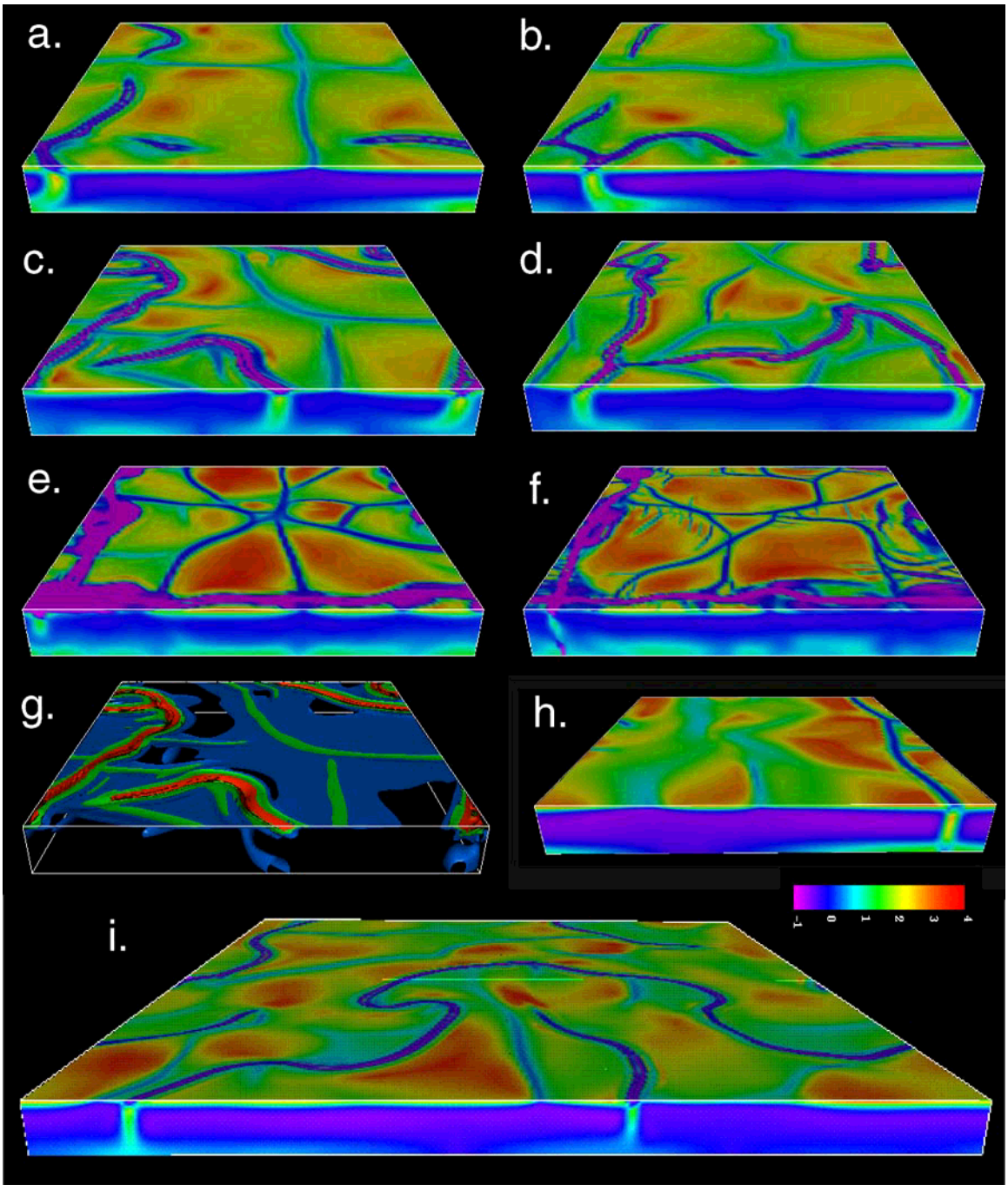

spheric volume also leads to an increase in surface poloidal motion and a decrease in deep-mantle poloidal motion. As a result, toroidal:poloidal ratio does not increase. It appears that plate motion is increasingly decoupled from deep mantle motion as the asthenosphere becomes more pervasive, as expected.

[71] Depth-dependent viscosity (Figure 14c) only slightly modifies the depth distribution of toroidal and poloidal motions. Toroidal motion now decreases with depth by, if anything, a smaller amount than before. Poloidal motion is now larger at the surface than the CMB, because of the lower viscosity at the surface. With evolving damage (Figure 14d) both toroidal and poloidal components are larger at the surface than in the deep mantle.

[72] In conclusion, toroidal motion is not restricted to shallow regions, and there can be substantial deep-mantle toroidal motion, at least in these simple models. A greater, more realistic viscosity increase with depth is likely to reduce deep toroidal motion.

4. Discussion and Conclusions

[73] As in paper 1 [*Tackley*, 2000b], many of the presented cases display smoothly evolving platelike behavior that is continuous in space and time and bears some crude resemblance to Earth's plate tectonics, though with some important differences. Some major successes of these models are the presence of very long wavelength flow with linear downwellings, the robust presence of passive spreading centers, and toroidal:poloidal ratios that are in the range observed for Earth (despite a lack of pure transform boundaries). Sometimes, single-sided subduction is observed although more commonly it is double-sided.

[74] This paper adds two rheological complexities to the model of paper 1: an asthenosphere and strain weakening. Both are found to enhance the quality of platelike behavior, in some cases, substantially. In this section the main findings are summarized, implications for Earth and other planets are discussed, and directions for future work are identified.

4.1. General Findings

4.1.1. Asthenosphere

[75] Using a melting viscosity reduction (MVR) criterion (i.e., introducing an asthenosphere by reducing the viscosity by a factor of 10 where material reaches a solidus) dramatically improves plate quality, as is evident both visually and from the "plateness" diagnostic, which jumps from ~0.7 to ~0.9. There is little difference in plate quality between models where this asthenosphere is restricted to the vicinity of spreading centers and models where it forms a global, upper-mantle-like layer, indicating that lubrication of spreading centers is the key process for improving plate behavior. Good, smoothly evolving platelike behavior is obtained over a wide range of yield stress values spanning an order of magnitude, unlike previous results where the best plate behavior occurred over a narrow range of yield strength. Quantitatively, platelike behavior was obtained between $\sigma_y = 1.4 \times 10^3$ and 1.4×10^4, scaling to between 17 and 170 MPa. It is possible that a negative feedback mechanism operates in this range: higher yield stress values result in slower plates and hence higher internal temperatures,

Figure 10. Cases with evolving damage (SWTH) or strain-rate weakening (SRW) and a composite yield stress of 1.4×10^4. Figures 10a–10f show a comparison of SWTH (left) with SRW (right) with the magnitude of damage or SRW increasing from top to bottom, as indicated by "maximum" stress (equation (12)) of (Figures 10a and 10b) 1.4×10^4; (Figures 10c and 10d) $\sigma_y = 5.7 \times 10^3$; and (Figures 10e and 10f) $\sigma_y = 2.8 \times 10^3$. (Figure 10g) The distribution of damage for the case in Figure 10c. Isocontours show D = 0.1 (blue), 0.5 (green), and 0.9 (red). (Figure 10h) Reference case with no strain weakening of any type. (Figure 10i) As in Figure 10a but in a $16 \times 16 \times 1$ domain.

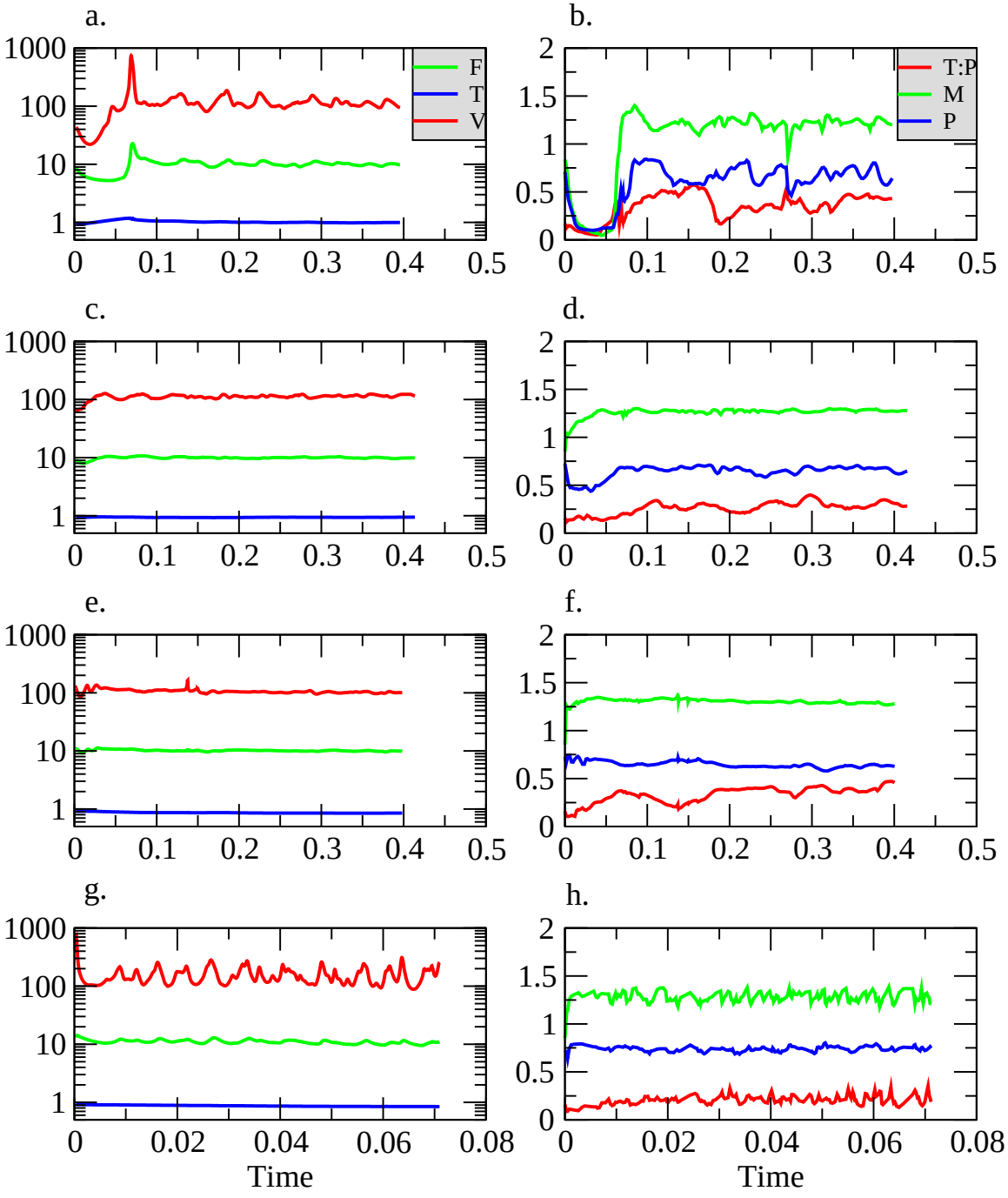
a.
b.
c.
d.
e.
f.
g.
h.
F
T
V
T:P
M
P
1000
100
10
1
2
1.5
0.5
0
0.1
0.2
0.3
0.4
0.5
0.02
0.04
0.06
0.08
Time

which then produces more melt-induced "lubrication," speeding plates up again.

[76] Bimodal stable solutions are obtained over a range of yield stresses; that is, either immobile-lid or plate behavior may be obtained, depending on initial condition. It appears that the thick global low-viscosity layer that forms under the rigid lid because of high temperatures prevents high enough stresses for lid breakage to occur. This finding could be very important for understanding planetary evolution.

[77] By contrast, introducing an asthenosphere by using depth-dependent viscosity has a smaller effect on system behavior, at least for the factor of 10 increase considered here. With larger, more realistic depth-viscosity increases the effect would of course be greater, but the intent here is to compare the two methods using the same amount of viscosity change.

4.1.2. Strain weakening

[78] Strain weakening plus time healing (SWTH) and strain-rate weakening (SRW) lubricate both convergent zones and spreading centers, the former more so. At spreading centers, localization is improved, but increasing prevalence of weakening leads to an increasingly complex network of spreading centers that fragment the plates in a manner resembling cracked glass. Convergent zones near downwellings are substantially weakened and widened, which can make downwellings highly episodic. Moderate amounts of strain weakening reduce time variability, but large amounts can make the system more time variable. SWTH or SRW does not lead to pure transform boundaries in these calculations and seems to have little systematic effect on the toroidal:poloidal ratio and only a moderate improvement effect on plateness. Time-dependent damage evolution and instantaneous strain-rate weakening produce very similar results. In some cases with moderate weakening, single-sided subduction is often observed.

4.1.3. Physical interpretation

[79] Why is MVR much more effective in improving plate quality than purely depth-dependent viscosity or SRW? A possible explanation for this is as follows: There is an imbalance between convergent plate boundaries and divergent plate boundaries (spreading centers); convergent boundaries form and continue easily because of the localized buoyancy of downwellings, whereas passive spreading centers have difficulty in forming and continuing. Introducing depth-dependent viscosity everywhere affects convergent zones and spreading centers equally, and introducing strain weakening lubricates convergent zones more than spreading centers. Only melt viscosity reduction lubricates spreading centers without affecting convergent zones. Thus MVR is the most effective complexity in redressing the imbalance in forming and maintaining convergent and divergent plate boundaries. This is consistent with the finding of *Zhong et al.* [1998], although those authors were focusing on the lubrication of pure transform boundaries, whereas here the lubrication is of spreading centers.

Figure 11. Time series of flow diagnostics (left column) and plate diagnostics (right column) for cases with evolving damage and composite yield stress 1.4×10^4. Flow diagnostics are mean temperature (blue), surface heat flux (green), and rms velocity (red). Plate diagnostics are plateness (blue), mobility (green), and toroidal:poloidal ratio (red). (Figures 11a–11b) Reference case with no strain weakening; (Figures 11c and 11d) $\sigma_{max} = 1.4 \times 10^4$; (Figures 11e and 11f) $\sigma_{max} = 5.7 \times 10^3$; and (Figures 11g and 11h) $\sigma_{max} = 2.8 \times 10^3$.

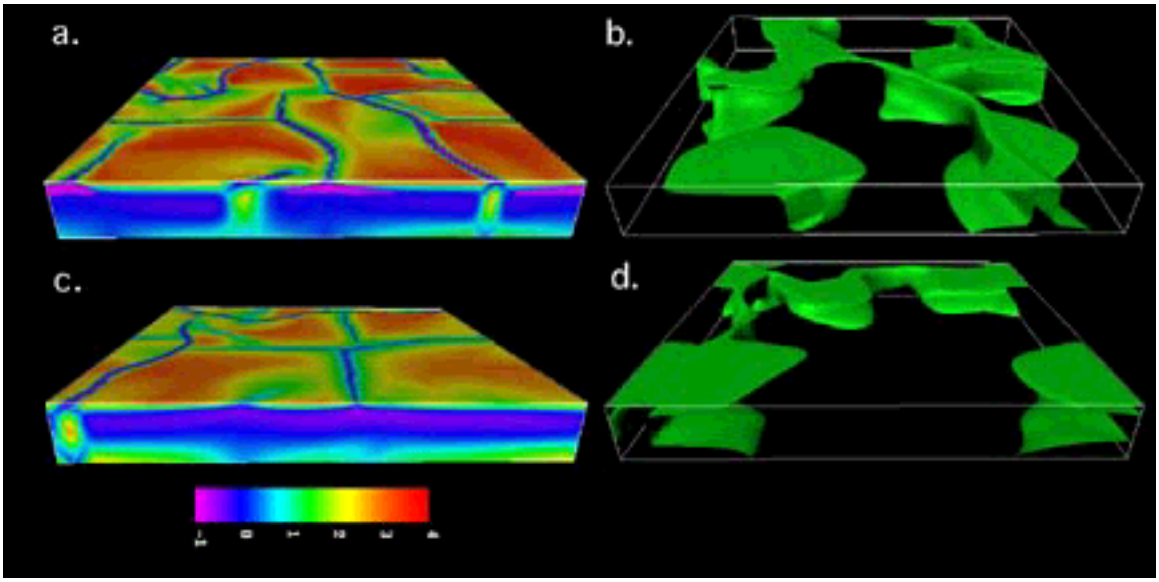

Figure 12. Cases with both strain-rate weakening and either melt viscosity reduction or depth-dependent viscosity. (Figures 12a and 12b) Constant $\sigma_y = 8.5 \times 10^3$ plus MVR with $T_{sol0} = 0.6$ plus SRW with $\sigma_{max} = 5.7 \times 10^3$. (Figures 12c and 12d) Composite $\sigma_y = 1.4 \times 10^4$ plus depth-dependent viscosity factor 10 plus SRW with $\sigma_{max} = 1.4 \times 10^4$. The color bar shows log10(viscosity), which varies between 0.1 and 10,000. The horizontal viscosity slice is at $z = 0.97$.

4.1.4. Toroidal, poloidal

[80] The cases presented here and in paper 1 show that regardless of which physical complexities are included, cases exhibiting good platelike behavior also display toroidal:poloidal ratios in the range observed for the Earth during the last 120 million years (0.3–0.5 [*Lithgow-Bertelloni et al.*, 1993]). Indeed, the addition of an asthenosphere or strain weakening does not appear to enhance the toroidal:poloidal ratio and sometimes reduces it. Toroidal energy decreases with depth, but the decrease seems to occur in a restricted depth interval and is only a factor of ~2 in the absence of an asthenosphere. An asthenosphere reduces deep-mantle toroidal motion and increases surface toroidal motion; however, it also enhances surface poloidal motion, so the ratio is not much affected.

4.2. Implications for Earth and Other Planets

4.2.1. Earth versus Venus

[81] From these results it appears that the existence of a low-viscosity layer beneath oceanic plates plays a large role in facilitating Earth-like plate tectonics. Neither a global asthenosphere nor dramatic viscosity reduction seems necessary: a factor of 10 viscosity decrease restricted to the regions around spreading centers is sufficient, at least in the parameter range studied here. From this result it is tempting to hypothesize that a reason for Venus not having plate tectonics is the commonly held belief that Venus does not have an asthenosphere, which is generally attributed to a lack of water [*Kaula*, 1994]. However, this interpretation must be treated with caution for the following reasons: (1) Even without melting there will still be a

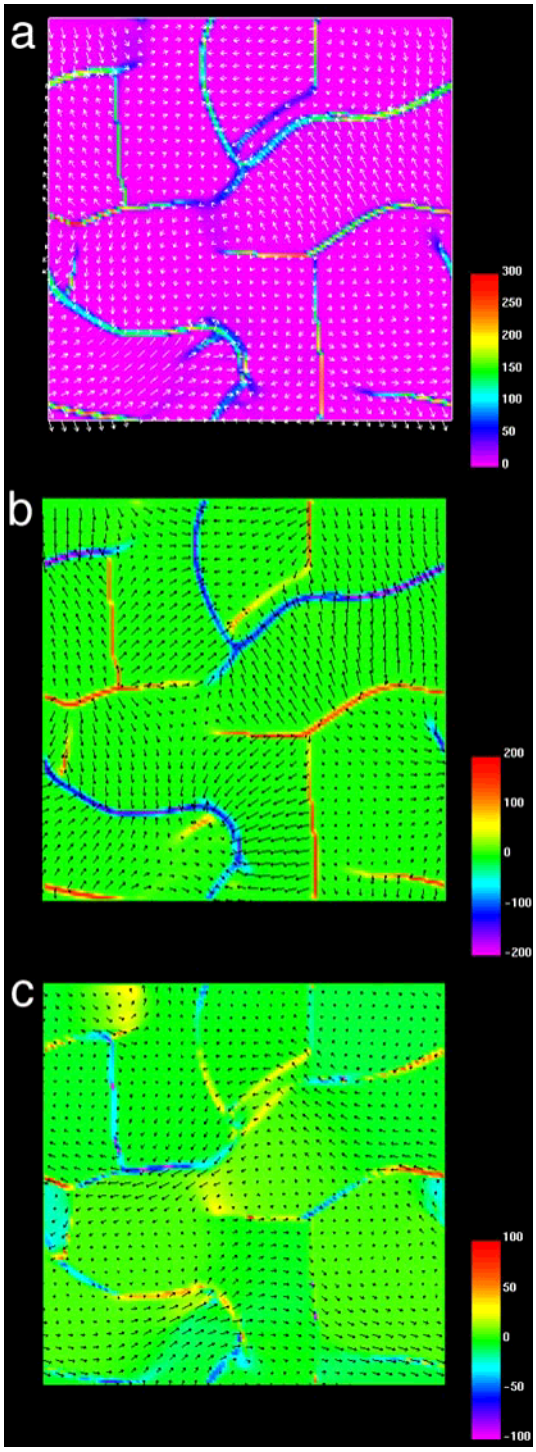

close approach of the venotherm to the dry solidus because the dry solidus has a steeper gradient than the adiabat; this should be sufficient to generate a limited asthenosphere. (2) With rigid-lid convection, Venus's interior should heat up enough to exceed even the dry solidus at sublithospheric depths [*Solomatov and Moresi*, 1996]. (3) The convection models in paper 1 show that platelike surface mobility can still occur with no asthenosphere, but it tends to be much more episodic. Another possibility from the present results is that Earth and Venus are simply an example of the observed bimodality of solutions: Venus is stuck in the immobile-lid mode, whereas Earth is stuck in the plate mode. However, it is probable that differences in lithospheric strength (rather than asthenospheric strength) are the key: the lack of water at the surface will dramatically increase both the crustal and lithospheric viscosity [*Hirth and Kohlstedt*, 1996] and the friction on faults because of an absence of pore pressure.

4.2.2. Horizontal wavelengths

[82] In paper 1 it was noted that all cases displaying mobile lithospheres also display a very long wavelength pattern of downwellings and hence long-wavelength mantle heterogeneity. This finding also holds true for the cases presented in this paper. Previous studies without plates have suggested various mechanisms for creating long-wavelength heterogeneity in the mantle, particularly depth-dependent viscosity and/or other parameters [*Bunge et al.*, 1996;

Figure 13. Decomposition of surface velocity field into toroidal and poloidal components for the case with constant $\sigma_y = 8.5 \times 10^3$ plus MVR with $T_{sol0} = 0.6$ plus SRW with $\sigma_{max} = 5.7 \times 10^3$ illustrated in Figures 12a and 12b: (a) total surface velocity field and surface strain rate, (b) poloidal velocity field and horizontal divergence, and (c) toroidal velocity field and vertical vorticity.

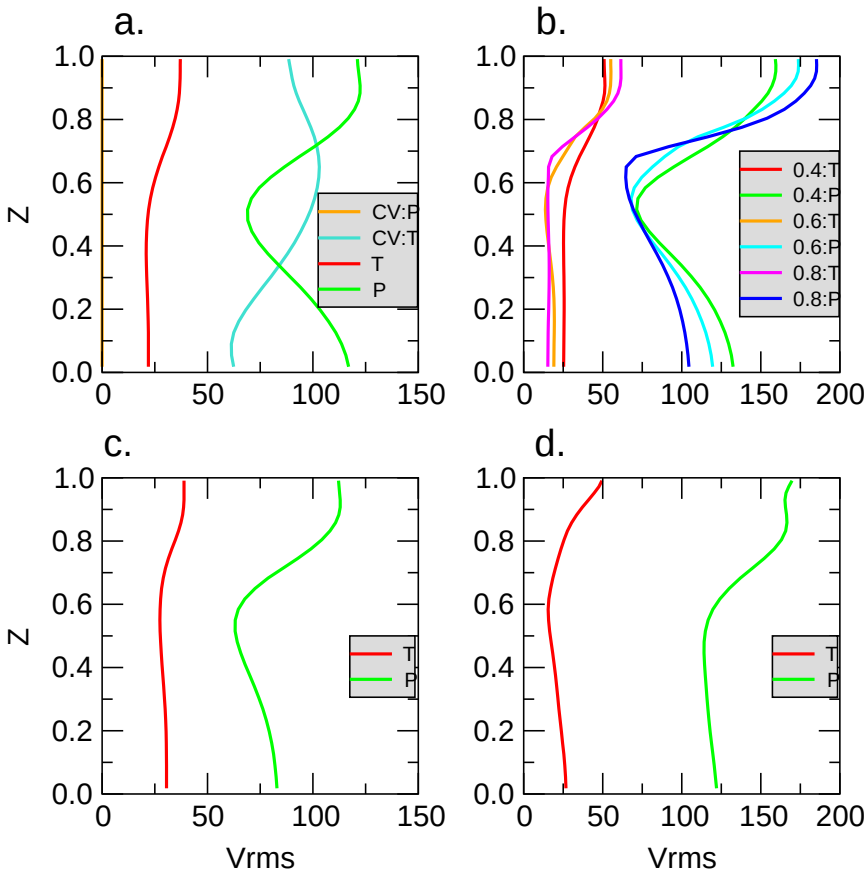

Figure 14. Radial profiles of rms poloidal and toroidal velocities for selected cases with constant yield stress 8.5×10^3: (a) reference case with no additional complexities (red, toroidal; green, poloidal) compared to constant-viscosity case (turquoise), (b) cases with melting viscosity reduction affecting increasingly large regions; $T_{sol0} = 0.8$ (red, toroidal; green, poloidal), 0.6 (orange, toroidal; turquoise, poloidal), 0.4 (magenta, toroidal; blue, poloidal), (c) with depth-dependent viscosity factor 10 (red, toroidal; green, poloidal), and (d) with evolving damage $\sigma_{max} = 2.8 \times 10^3$ (red, toroidal; green, poloidal).

Hansen et al., 1993], continental motions [*Gurnis and Zhong*, 1991; *Zhong and Gurnis*, 1993], and the endothermic phase transition at 660 km depth [*Tackley*, 1995; 1996b; *Tackley et al.*, 1993]. The results presented here and in paper 1 seem to indicate that long-wavelength flow is a natural consequence of a mobile but high-viscosity lid, with no other complexity being necessary. However, this needs to be verified for higher Rayleigh numbers (which lead to shorter-wavelength structure [*Tackley*, 1996b]) and higher viscosity contrasts.

4.2.3. Model shortcomings

[83] The most notable shortcomings of these models with respect to obtaining Earth-like dynamics (other than the obvious lack of continents) are the pervasiveness of double-sided (symmetric) subduction, the lack of pure transform boundaries, and the low convective vigor (heat flux). Some discussion of this was presented in paper 1. In the new results presented here it is interesting that (1) single-sided (asymmetric) subduction is common in some of the

cases with strain weakening and (2) ridge offsets are observed in some of the cases with melting viscosity reduction, although the ridge offsets are not perfectly perpendicular to the ridge. These findings suggest directions for future investigation, although it may be that actual brittle failure at shallow depths is necessary to generate at least the spreading center transform faults. The present cases do not display long-term history dependence such as reactivation of old weak zones that is observed on Earth [*Gurnis et al.*, 2000]; this is something that requires continents and a more realistic rheology.

4.3. Yielding Versus Strain Weakening

[84] In these results, pseudoplastic yielding with no strain weakening is effective in generating weak, localized plate boundaries. This seems contrary to expectations from previous modeling results [*Bercovici*, 1995, 1998; *Tackley*, 1998, 2000a], in which it appeared that self-lubricating (e.g., strain-rate-weakening) rheology was necessary to form plate tectonics in three dimensions. It is possible to reconcile these apparently contradictory findings by noting that the earlier studies focused on the formation of transform boundaries as an essential component of plate behavior, whereas in the present results, platelike behavior is obtained without pure transform boundaries being necessary. Thus, while self-lubrication is necessary for the formation of focused pure transform boundaries, focused pure transform boundaries are not (at the large scale) necessary for plate tectonics. A robust result from previous work is thus that some form of strain weakening is necessary to obtain transform boundaries, which leads to the question: Why don't transform boundaries form in the presented cases where strain weakening is included? Increasing the amount of strain weakening does not seem to help because this leads to high episodicity and runaway events (i.e., rapid collapse of large regions of the lithosphere near downwellings into the mantle). It is difficult to simultaneously get non-runaway downwellings and localized strike-slip boundaries. It could be that the damage evolution model does not adequately represent the important physics, including, perhaps, brittle failure.

4.4. The Persistence of Memory?

[85] Geological observations indicate that on Earth, long-lived "preexisting" zones of weakness are important in the plate tectonic process, often forming the sites of "new" plate boundaries (for a summary, see *Gurnis et al.* [2000]). In the present results, however, first-order platelike behavior is obtained with an "instantaneous" rheological description, and when history dependence is introduced in the form of evolving damage, it does not appear to make a first-order difference compared to an equivalent instantaneous parameterization. Thus it is important to reconcile the present results with geological observations and identify important areas where the present description should be improved.

[86] One key shortcoming of the presented models is that they contain only oceanic lithosphere and no continents. On Earth, continental lithosphere is essential for retaining memory for billions of years, since oceanic lithosphere has a maximum age of only ~200 million years. Furthermore, oceanic plates form at spreading centers and do not have much opportunity to build up deformation history until they reach subduction zones (as occurs in the presented models, where the produced "damage" is immediately advected into the mantle). As pointed out by *Gurnis et al.* [2000], oceanic plates are strong and rigid enough to support the stress associated with 9 km high oceanic islands in their interiors but at subduction zones deform with an effective

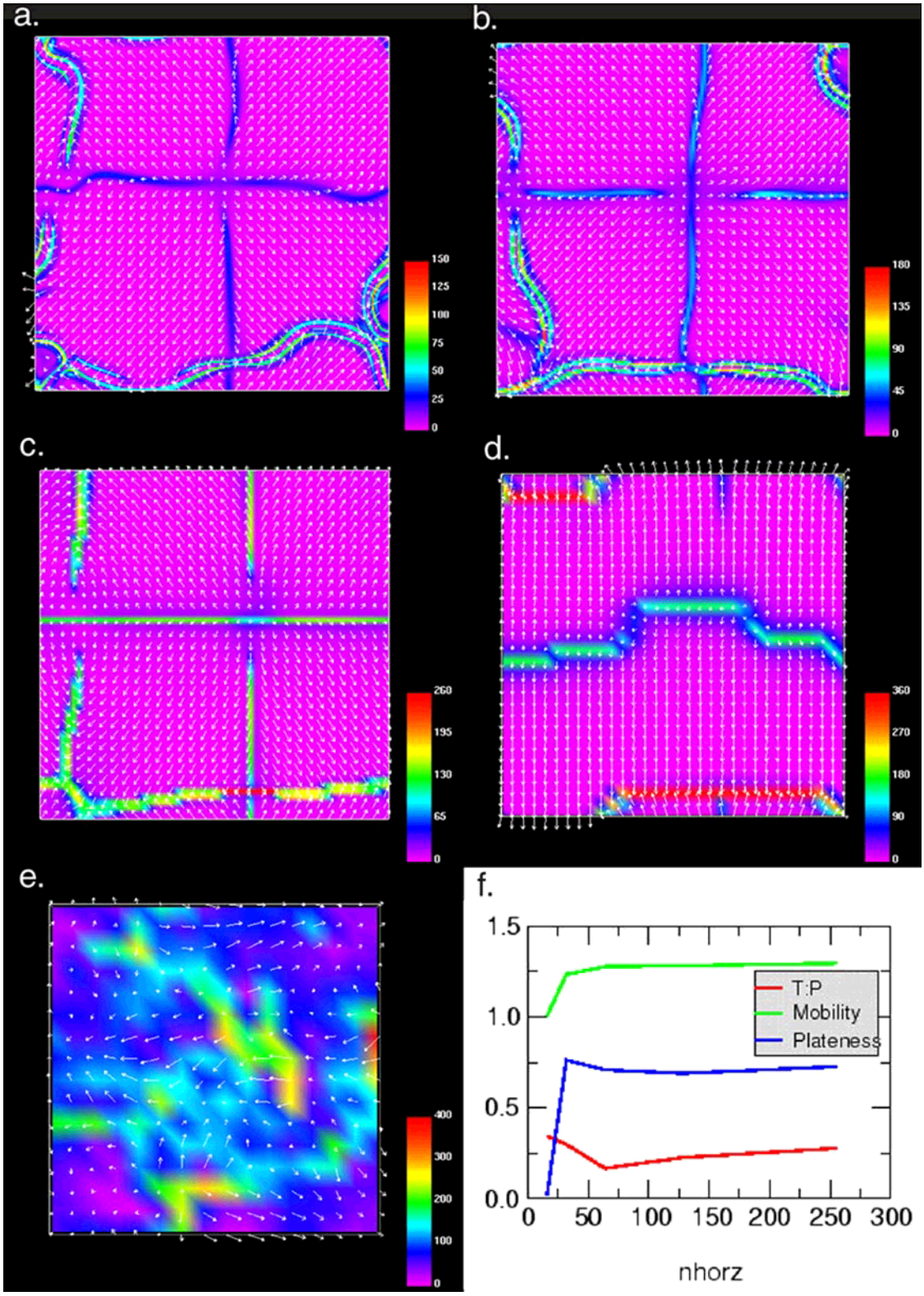
a.
150
125
100
75
50
25
0
b.
180
135
90
45
0
c.
260
195
130
65
0
d.
360
270
180
90
0
e.
400
300
200
100
0
f.
1.5
1.0
0.5
0.0
0
50
100
150
200
250
300
nhorz
T:P
Mobility
Plateness

viscosity that is almost as low as the viscosity of regular upper mantle material. The bending of subducting slabs may be a situation where memory is of little importance and an instantaneous rheological description is appropriate, although the lubrication of subduction shear zone by advected weak sediments [*Cloos and Shreve*, 1988a, 1988b; *Lenardic and Kaula*, 1994], associated metamorphism, and possibly fluid overpressure [*Peacock*, 1990a, 1990b] requires a more complex treatment. Oceanic fracture zones may, however, be a type of feature that requires history-dependent weakening and is sometimes important in the plate tectonic process. Mid-ocean ridge transform faults and thus fracture zones may be substantially weakened by serpentinization [*Escartin et al.*, 1997a, 1997b] and are often observed to be nucleation sites for new plate boundaries [*Gurnis et al.*, 2000]. Transform faults appear to form in the brittle regime; thus brittle failure and hydration-related weakening may be important processes to include in future modeling. Undoubtedly, there are other limitations to the present weakening model, since it does not represent a specific process, and rheological parameters in general must be scaled back from realistic values. For example, with the limited viscosity contrast modeled here the simultaneous specification of realistic very long healing timescales at low temperature, and reasonable strains for weakening (equation (10)), leads to runaway behavior because damage is produced too rapidly relative to healing.

[87] Obviously, new plate boundaries will preferentially form along any suitable preexisting lines of weakness that may be present, as observed in the field. The key question to address in the future is not whether such weak zones play an important role, but whether they are necessary for Earth-like plate tectonics. Specifically, does the very existence of Earth's present plate tectonic regime depend on the ability of the lithosphere to retain long-term memory of weakness, or is the reuse of already weakened areas merely a convenience? An implicit assumption in most previous studies of plate generation has been the latter [e.g., *Moresi and Solomatov*, 1998; *Tackley*, 1998; *Weinstein and Olson*, 1992]; however, as in the present study, only oceanic lithosphere, the component of Earth's plate tectonics least affected by long-term memory, was modeled.

[88] Arguing in favor of the "convenience" view is the finding that even in simulations with purely instantaneous rheology, plate boundaries often persist over long time periods and always evolve continuously. They do not instantaneously appear and disappear out of nowhere in one time step. New rifts or subduction zones take a finite amount of time to form and propagate, even in the highly time-dependent "erratic" cases. Thus the long-term persistence of active plate boundaries on Earth is not a strong argument for the importance of memory. Of course, the temperature field is a function of previous deformation history and thus gives the system a type of memory.

[89] Arguing in favor of the "necessary" view is the finding from the present simulations and previous constraints (see paper 1) that in order for plates to exist, the effective strength of the oceanic lithosphere must be lower by a factor

Figure 15. Effect of numerical resolution on surface deformation for composite yield stress 1.4×10^4 and evolving damage with $\sigma_{max} = 1.4 \times 10^4$. The number of grid cells is (a) $256 \times 256 \times 64$, (b) $128 \times 128 \times 32$, (c) $64 \times 64 \times 16$, (d) $32 \times 32 \times 8$, and (e) $16 \times 16 \times 4$. Strain rate values were calculated assuming grid spacing equal to 1, so they must be appropriately scaled if intercomparison is desired. (f) The scaling of time-averaged plate diagnostics with resolution.

of ~4–5 than the strength of rocks to semi-brittle or low-temperature plastic deformation measured by laboratory experiments [*Kirby*, 1980; *Kohlstedt et al.*, 1995]. This discrepancy could be explained if lithospheric "failure" actually takes place in zones that have already been substantially weakened by plate boundary processes in the past. However, such arguments do not seem capable of explaining the low strength of previously undamaged oceanic lithosphere as it bends in the subduction zone, implying that our understanding of how laboratory results apply to the real Earth is incomplete [*Rutter and Brodie*, 1991].

[90] In summary, the finding that the present parameterization of history-dependent weakening does not have a large effect on oceanic plate dynamics is not surprising but does not imply that history-dependent deformation is unimportant in Earth. The central issue of whether weak zone reactivation is a necessity or just a convenience will require much research to resolve.

4.5. Future Directions

[91] It is possible to make a long "shopping list" of improvements that could be made to the present model, the most important of which may be the inclusion of continents (both crust and cratonic lithosphere) and the inclusion of actual brittle failure (not a parameterization using depth-dependent viscoplastic yielding) in the shallow region, which may be the behavior needed to obtain transform segments.

[92] Various desired improvements to the rheological model include adding other deformation mechanisms that are known about (power-law dislocation creep, the Peierls mechanism), bringing rheological parameters such as activation energies closer to Earth-like (although this requires a more robust numerical solution scheme and *Moresi and Solomatov* [1998] found only a weak sensitivity to viscosity contrast for 2-D models), as well as various complexities such as a viscosity increase after oceanic lithosphere loses its melt, which may help to make oceanic plates more rigid. Furthermore, it will be necessary to include actual weakening mechanisms observed in nature, such as grain-size reduction. The use of a compressible rather than Boussinesq formulation would open the possibility of shear zone formation through viscous heating. A general problem with including mechanisms that lead to strong localization is that of resolving the resulting small-scale features, perhaps requiring techniques such as adaptive grid refinement.

[93] A convective regime (heat flux and velocities) closer to Earth-like could be straightforwardly accomplished using higher resolution, and this is the subject of the next paper ("paper 3," in preparation), although from previous, two-dimensional work [*Moresi and Solomatov*, 1998; *Richards et al.*, 1999], first-order differences in the dynamics are not expected. Spherical geometry will ultimately be necessary, although preliminary results in spherical geometry (J. R. Baumgardner, personal communication, 1999) show results very similar to some of those reported here. The effects of the believed small fraction of basal heating (10–20%) may be important in some circumstances, such as initiating rifting.

Appendix A: Resolution Test

[94] Since many of these cases contain very narrow features with very large viscosity contrasts, it is natural to ask whether the numerical resolution is sufficient, or whether it may be affecting the results in some way. To investigate this, two of the cases were run at a series of additional resolutions, namely, $16 \times 16 \times 4$, $32 \times 32 \times 8$, $64 \times 64 \times 16$, and $256 \times 256 \times$

64 (the standard resolution was 128 × 128 × 32). Surface deformation results for one case (the "strain-weakening" case with composite $\sigma_y = 1.4 \times 10^4$) are presented in Figure 15, with scaling of plate diagnostics indicated in Figure 15f.

[95] Comparing the double resolution version (Figure 15a) with the standard resolution case (Figure 15b) reveals little change, suggesting that the standard resolution is sufficient. Degrading the resolution by a factor of 2 (Figure 15c) results in little change to the overall pattern, but weak zones now appear to have grid-limited widths and often follow the grid directions. Remarkably, platelike behavior is still obtained even with a further factor of 2 reduction (to 32 × 32 × 8), but the solution certainly looks grid-limited. The solution is lost with a final factor of 2 reduction (to 16 × 16 × 4). Diagnostics of plate behavior (Figure 15f) are roughly constant with resolution except for at the extremely coarse grid.

[96] It is surprising that both the character of the solution and quantitative plate diagnostics are robust down to very low resolutions, when benchmarks [*Blankenbach et al.*, 1989; *Travis et al.*, 1990] indicate a need for several grid points in the boundary layers to get accurate results even for simple rheologies. This indicates that the plate diagnostics used are sensitive to the large-scale structure of the flow, not local accuracy. In addition, the width of weak zones seems to scale with boundary layer thickness, so the fairly low heat flow in the present results helps. The standard resolution, which includes vertical grid refinement in the upper boundary layer, does result in several grid cells across convective features: there are 5–6 vertical cells over the lithosphere, and since downwellings are generally double-sided, they are at least twice as wide as the upper boundary layer thickness, so higher horizontal grid spacing is appropriate.

[97] In conclusion, the general character of platelike behavior, and quantitative values of global diagnostics, are reproduced on amazingly coarse grids, as little as 1/4 the resolution of the standard grid used in this paper. "Challenged" resolution is indicated by weak zones 1 cell wide that follow grid lines.

Acknowledgments

[98] This research was supported by a NASA/HPCC grant and the David and Lucile Packard Foundation. Useful discussions were had with Shun Karato, Greg Hirth, David Bercovici, and John Baumgardner. Reviews by Mike Gurnis, Peter van Keken, and Greg Hirth improved the manuscript.

References

Bercovici, D., A simple model of plate generation from mantle flow, *Geophys. J. Int.*, *114*(3), 635–650, 1993.

Bercovici, D., A source-sink model of the generation of plate tectonics from non-Newtonian mantle flow, *J. Geophys. Res.*, *100*(B2), 2013–2030, 1995.

Bercovici, D., Plate generation in a simple model of lithosphere-mantle flow with dynamic self-lubrication, *Earth Planet. Sci. Lett.*, *144*(1–2), 41–51, 1996.

Bercovici, D., Generation of plate tectonics from lithosphere-mantle flow and void-volatile self-lubrication, *Earth Planet. Sci. Lett.*, *154*, 139–151, 1998.

Bercovici, D., Y. Ricard, and M. A. Richards, The relation between mantle dynamics and plate tectonics: A primer, in *Geophysical Monograph Series*, edited by M. A. Richards, R. Gordon, and R. van der Hilst, AGU, Washington, D. C., in press, 2000.

Blankenbach, B., F. Busse, U. Christensen, L. Cserepes, D. Gunkel, U. Hansen, H. Harder, G. Jarvis, M. Koch, G. Marquart, D. Moore, P. Olson, H. Schmeling, and T. Schnaubelt, A benchmark comparison for mantle convection codes, *Geophys. J. Int.*, *98*(1), 23–38, 1989.

Braun, J., J. Chery, A. Poliakov, D. Mainprice, A. Vauchez, A. Tomassi, and M. Daignieres, A simple parameterization of strain localization in the ductile regime due to grain size reduction: A case study for olivine, *J. Geophys. Res.*, *104*(B11), 25,167–25,181, 1999.

Bunge, H. P., and M. A. Richards, The origin of large-scale structure in mantle convection—Effects of plate motions and viscosity stratification, *Geophys. Res. Lett.*, *23*(21), 2987–2990, 1996.

Bunge, H. P., M. A. Richards, and J. R. Baumgardner,

Effect of depth-dependent viscosity on the planform of mantle convection, *Nature*, *379*(6564), 436–438, 1996.

Byerlee, J., The brittle-ductile transition in rocks, *J. Geophys. Res.*, *73*, 4741–4750, 1968.

Christensen, U., Convection with pressure-dependent and temperature-dependent non-Newtonian rheology, *Geophys. J. R. Astron. Soc.*, *77*(2), 343–384, 1984a.

Christensen, U. R., Heat transport by variable viscosity convection and implications for the Earth's thermal evolution, *Phys. Earth Planet. Inter.*, *35*(4), 264–282, 1984b.

Cloos, M., and R. L. Shreve, Subduction-channel model of prism accretion, melange formation, sediment subduction, and subduction erosion at convergent plate margins, part 1, Background and description, *Pure Appl. Geophys.*, *128*(3–4), 455–500, 1988a.

Cloos, M., and R. L. Shreve, Subduction-channel model of prism accretion, melange formation, sediment subduction, and subduction erosion at convergent plate margins, part II, Implications and discussion, *Pure Appl. Geophys.*, *128*(3–4), 501–545, 1988b.

Cloos, M., and R. L. Shreve, Shear-zone thickness and the seismicity of Chilean- and Marianas-type subduction zones, *Geology*, *24*(2), 107–110, 1996.

Cserepes, L., Numerical studies of non-Newtonian mantle convection, *Phys. Earth Plan. Inter.*, *30*(1), 49–61, 1982.

Davies, G. F., Mantle convection model with a dynamic plate—Topography, heat flow and gravity anomalies, *Geophys. J. Int.*, *98*(3), 461–464, 1989.

Drury, M. R., R. L. M. Vissers, D. Vanderwal, and E. H. H. Strating, Shear localization in upper mantle peridotites, *Pure Appl. Geophys.*, *137*(4), 439–460, 1991.

Escartin, J., G. Hirth, and B. Evans, Effects of serpentinization on the lithospheric strength and the style of normal faulting at slow-spreading ridges, *Earth Planet. Sci. Lett.*, *151*(3–4), 181–189, 1997a.

Escartin, J., G. Hirth, and B. Evans, Nondilatant brittle deformation of serpentinites: Implications for Mohr-Coulomb theory and the strength of faults, *J. Geophys. Res.*, *102*(B2), 2897–2913, 1997b.

Fleitout, L., and C. Froidevaux, Thermal and mechanical evolution of shear zones, *J. Struct. Geol.*, *2*, 159–164, 1980.

Gable, C. W., R. J. O'Connell, and B. J. Travis, Convection in three dimensions with surface plates: Generation of toroidal flow, *J. Geophys. Res.*, *96*(B5), 8391–8405, 1991.

Govers, R., and M. J. R. Wortel, Extension of stable continental lithosphere and the initiation of lithospheric scale faults, *Tectonics*, *14*(4), 1041–1055, 1995.

Gurnis, M., and S. Zhong, Generation of long wavelength heterogeneity in the mantle by the dynamic interaction between plates and convection, *Geophys. Res. Lett.*, *18*(4), 581–584, 1991.

Gurnis, M., S. Zhong, and J. Toth, On the competing roles of fault reactivation and brittle failure in generating plate tectonics from mantle convection, in *Geophysical Monograph Series*, edited by M. A. Richards, R. Gordon, and R. van der Hilst, AGU, Washington, D. C., in press, 2000.

Hager, B. H., and R. J. O'Connell, Subduction zone dip angles and flow driven by plate motion, *Tectonophysics*, *50*, 111–133, 1978.

Hansen, U., D. A. Yuen, S. E. Kroening, and T. B. Larsen, Dynamic consequences of depth-dependent thermal expansivity and viscosity on mantle circulations and thermal structure, *Phys. Earth Planet. Inter.*, *77*(3–4), 205–223, 1993.

Hirth, G., and D. L. Kohlstedt, Water in the oceanic upper-mantle—Implications for rheology, melt extraction and the evolution of the lithosphere, *Earth Planet. Sci. Lett.*, *144*(1–2), 93–108, 1996.

Jaroslow, G. E., G. Hirth, and H. J. B. Dick, Abyssal peridotite mylonites—Implications for grain-size sensitive flow and strain localization in the oceanic lithosphere, *Tectonophysics*, *256*(1–4), 17–37, 1996.

Jin, D. H., S. Karato, and M. Obata, Mechanisms of shear localization in the continental lithosphere—Inference from the deformation microstructures of peridotites from the Ivrea zone, northwestern Italy, *J. Struct. Geol.*, *20*(2–3), 195–209, 1998.

Kameyama, M., D. A. Yuen, and H. Fujimoto, The interaction of viscous heating with grain-size dependent rheology in the formation of localized slip zones, *Geophys. Res. Lett.*, *24*(20), 2523–2526, 1997.

Kaula, W. M., The tectonics of Venus, *Philos. Trans. R. Soc. London, Ser. A*, *349*(1690), 345–355, 1994.

King, S. D., and B. H. Hager, Subducted slabs and the geoid, 1, Numerical experiments with temperature-dependent viscosity, *J. Geophys. Res.*, *99*(B10), 19,843–19,852, 1994.

Kirby, S. H., Tectonic stresses in the lithosphere: Constraints provided by the experimental deformation of rocks, *J. Geophys. Res.*, *85*(B11), 6353–6363, 1980.

Kohlstedt, D. L., B. Evans, and S. J. Mackwell, Strength of the lithosphere: Constraints imposed by laboratory experiments, *J. Geophys. Res.*, *100*(B9), 17,587–17,602, 1995.

Kopitzke, U., Finite element convection models: Comparison of shallow and deep mantle convection, and temperatures in the mantle, *J. Geophys.*, *46*, 97–121, 1979.

Leloup, P. H., Y. Ricard, J. Battaglia, and R. Lacassin, Shear heating in continental strike-slip shear zones: Model and field examples, *Geophys. J. Int.*, *136*(1), 19–40, 1999.

Lenardic, A., and W. M. Kaula, Self-lubricated mantle

convection—2-dimensional models, *Geophys. Res. Lett.*, *21*(16), 1707–1710, 1994.

Lithgow-Bertelloni, C., M. A. Richards, Y. Ricard, R. J. O'Connell, and D. C. Engebretson, Toroidal-poloidal partitioning of plate motions since 120 Ma, *Geophys. Res. Lett.*, *20*(5), 375–378, 1993.

Marone, C., C. B. Raleigh, and C. H. Scholz, Frictional behavior and constitutive modeling of simulated fault gouge, *J. Geophys. Res.*, *95*(B5), 7007–7025, 1990.

Moresi, L., and V. Solomatov, Mantle convection with a brittle lithosphere—Thoughts on the global tectonic styles of the Earth and Venus, *Geophys. J. Int.*, *133*(3), 669–682, 1998.

O'Connell, R. J., and B. H. Hager, Toroidal-poloidal partitioning of lithospheric plate motions, in *Glacial Isostacy Sea-Level and Mantle Rheology*, pp. 535–551, Kluwer Acad., Norwell, Mass., 1991.

Ogawa, M., G. Schubert, and A. Zebib, Numerical simulations of 3-dimensional thermal convection in a fluid with strongly temperature-dependent viscosity, *J. Fluid Mech.*, *233*, 299–328, 1991.

Olson, P., and D. Bercovici, On the equipartition of kinetic energy in plate tectonics, *Geophys. Res. Lett.*, *18*(9), 1751–1754, 1991.

Parmentier, E. M., C. Sotin, and B. J. Travis, Turbulent 3-D thermal convection in an infinite Prandtl number, volumetrically heated fluid—Implications for mantle dynamics, *Geophys. J. Int.*, *116*(2), 241–251, 1994.

Peacock, S. M., Fluid processes in subduction zones, *Science*, *248*(4953), 329–337, 1990a.

Peacock, S. M., Numerical simulation of metamorphic pressure-temperature-time paths and fluid production in subducting slabs, *Tectonics*, *9*(5), 1197–1211, 1990b.

Peacock, S. M., and R. D. Hyndman, Hydrous minerals in the mantle wedge and the maximum depth of subduction thrust earthquakes, *Geophys. Res. Lett.*, *26*(16), 2517–2520, 1999.

Pili, E., Y. Ricard, J. M. Lardeaux, and S. M. F. Sheppard, Lithospheric shear zones and mantle-crust connections, *Tectonophysics*, *280*(1–2), 15–29, 1997.

Ratcliff, J. T., P. J. Tackley, G. Schubert, and A. Zebib, Transitions in thermal convection with strongly variable viscosity, *Phys. Earth Planet. Inter.*, *102*, 201–212, 1997.

Regenauer-Lieb, K., Dilatant plasticity applied to Alpine collision: Ductile void growth in the intraplate area beneath the Eifel volcanic field, *J. Geodyn.*, *27*(1), 1–21, 1999.

Regenauer-Lieb, K., and D. A. Yuen, Rapid conversion of elastic energy into plastic shear heating during incipient necking of the lithosphere, *Geophys. Res. Lett.*, *25*(14), 2737–2740, 1998.

Richards, M. A., W.-S. Yang, and J. R. Baumgardner, The effectiveness of finite yield stress in obtaining platelike surface velocities, *Eos Trans. AGU*, *80*(46), Fall Meet. Suppl., F962, 1999.

Rutter, E. H., and K. H. Brodie, Lithosphere rheology: A note of caution, *J. Struct. Geol.*, *13*(3), 363–367, 1991.

Rutter, E. H., R. E. Heilbronner, and H. E. Stuenitz, On the relationship between the formation of shear zones and the form of the flow law for rocks undergoing dynamic recrystallization, *Tectonophysics*, *303*(1–4), 147–158, 1999.

Schubert, G., and D. A. Yuen, Shear heating instability in the Earth's upper mantle, *Tectonophysics*, *50*, 197–205, 1988.

Sleep, N. H., and M. L. Blanpied, Creep, compaction and the weak rheology of major faults, *Nature*, *359*(6397), 687–692, 1992.

Solomatov, V. S., Scaling of temperature-dependent and stress-dependent viscosity convection, *Phys. Fluids*, *7*(2), 266–274, 1995.

Solomatov, V. S., and L. N. Moresi, Stagnant lid convection on Venus, *J. Geophys. Res.*, *101*(E2), 4737–4753, 1996.

Sorensen, K., Growth and dynamics of the Nordre-Stromfjord shear zone, *J. Geophys. Res.*, *88*(B4), 3419–3437, 1983.

Tackley, P. J., Effects of strongly temperature-dependent viscosity on time-dependent, 3-dimensional models of mantle convection, *Geophys. Res. Lett.*, *20*(20), 2187–2190, 1993.

Tackley, P. J., Three-dimensional models of mantle convection: Influence of phase transitions and temperature-dependent viscosity, Ph.D. thesis, Calif. Inst. of Technol., Pasadena, 1994.

Tackley, P. J., On the penetration of an endothermic phase transition by upwellings and downwellings, *J. Geophys. Res.*, *100*, 15,477–15,488, 1995.

Tackley, P. J., Effects of strongly variable viscosity on three-dimensional compressible convection in planetary mantles, *J. Geophys. Res.*, *101*, 3311–3332, 1996a.

Tackley, P. J., On the ability of phase transitions and viscosity layering to induce long-wavelength heterogeneity in the mantle, *Geophys. Res. Lett.*, *23*, 1985–1988, 1996b.

Tackley, P. J., Self-consistent generation of tectonic plates in three-dimensional mantle convection, *Earth Planet. Sci. Lett.*, *157*, 9–22, 1998.

Tackley, P. J., The quest for self-consistent incorporation of plate tectonics in mantle convection, in *Geophysical Monograph Series*, edited by M. A. Richards, R. Gordon, and R. van der Hilst, AGU, Washington, D. C., in press, 2000a.

Tackley, P. J., Self-consistent generation of tectonic plates in time-dependent, three-dimensional mantle convection simulations, 1, Pseudoplastic yielding, *Geochem. Geo-*

phys. Geosyst., *1* (Article) 2000GC000036 [14,503 words], August 23, 2000b.

Tackley, P. J., D. J. Stevenson, G. A. Glatzmaier, and G. Schubert, Effects of an endothermic phase transition at 670 km depth in a spherical model of convection in the Earth's mantle, *Nature*, *361*(6414), 699–704, 1993.

Thatcher, W., and P. C. England, Ductile shear zones beneath strike-slip faults: Implications for the thermomechanics of the San Andreas fault zone, *J. Geophys. Res.*, *103*(B1), 891–905, 1998.

Travis, B. J., C. Anderson, J. Baumgardner, C. W. Gable, B. H. Hager, R. J. O'Connell, P. Olson, A. Raefsky, and G. Schubert, A benchmark comparison of numerical-methods for infinite Prandtl number thermal-convection in 2-dimensional Cartesian geometry, *Geophys. Astrophys. Fluid Dyn.*, *55*(3–4), 137–160, 1990.

Trompert, R., and U. Hansen, Mantle convection simulations with rheologies that generate platelike behavior, *Nature*, *395*(6703), 686–689, 1998.

Trompert, R. A., and U. Hansen, The application of a finite-volume multigrid method to 3-dimensional flow problems in a highly viscous fluid with a variable viscosity, *Geophys. Astrophys. Fluid Dyn.*, *83*(3–4), 261–291, 1996.

Van den Berg, A. P., D. A. Yuen, and P. E. Van Keken, Effects of depth-variations in creep laws on the formation of plates in mantle dynamics, *Geophys. Res. Lett.*, *18*(12), 2197–2200, 1991.

Vissers, R. L. M., M. R. Drury, E. H. H. Strating, C. J. Spiers, and D. Vanderwal, Mantle shear zones and their effect on lithosphere strength during continental breakup, *Tectonophysics*, *249*(3–4), 155–171, 1995.

Weinstein, S. A., Thermal convection in a cylindrical annulus with a non-Newtonian outer surface, *Pure Appl. Geophys.*, *146*(3–4), 551–572, 1996.

Weinstein, S. A., The effect of convection planform on the toroidal-poloidal energy ratio, *Earth Planet. Sci. Lett.*, *155*(1–2), 87–95, 1998.

Weinstein, S. A., and P. L. Olson, Thermal convection with non-Newtonian plates, *Geophys. J. Int.*, *111*(3), 515–530, 1992.

Yuen, D. A., L. Fleitout, G. Schubert, and C. Froidevaux, Shear deformation zones along major transform faults and subducting slabs, *Geophys. J. R. Astron. Soc.*, *54*, 93–119, 1978.

Zhong, S., and M. Gurnis, Dynamic feedback between a continent-like raft and thermal convection, *J. Geophys. Res.*, *98*(B7), 12,219–12,232, 1993.

Zhong, S., and M. Gurnis, Towards a realistic simulation of plate margins in mantle convection, *Geophys. Res. Lett.*, *22*(8), 981–984, 1995.

Zhong, S., and M. Gurnis, Interaction of weak faults and non-Newtonian rheology produces plate-tectonics in a 3d model of mantle flow, *Nature*, *383*(6597), 245–247, 1996.

Zhong, S., M. Gurnis, and L. Moresi, Role of faults, nonlinear rheology, and viscosity structure in generating plates from instantaneous mantle flow models, *J. Geophys. Res.*, *103*(B7), 15,255–15,268, 1998.